The Astronomical Journal, 138:1969–1984, 2009 December doi:10.1088/0004-6256/138/6/1969
© 2009. The American Astronomical Society. All rights reserved. Printed in the U.S.A.

ASTROMETRY WITH THE *HUBBLE SPACE TELESCOPE*: TRIGONOMETRIC PARALLAXES OF PLANETARY NEBULA NUCLEI NGC 6853, NGC 7293, ABELL 31, AND DeHt 5*

G. Fritz Benedict[1], Barbara E. McArthur[1], Ralf Napiwotzki[2], Thomas E. Harrison[3], Hugh C. Harris[4], Edmund Nelan[5], Howard E. Bond[5], Richard J. Patterson[6], and Robin Ciardullo[7]
[1] McDonald Observatory, University of Texas, Austin, TX 78712, USA
[2] Centre for Astrophysics Research, STRI, University of Hertfordshire, College Lane, Hatfield AL10 9AB, UK
[3] Department of Astronomy, New Mexico State University, Las Cruces, NM 88003, USA
[4] United States Naval Observatory, Flagstaff Station, Flagstaff, AZ 86001, USA
[5] Space Telescope Science Institute, 3700 San Martin Dr, Baltimore, MD 21218, USA
[6] Department of Astronomy, University of Virginia, P.O. Box 3818, Charlottesville, VA 22903, USA
[7] Department of Astronomy and Astrophysics, Pennsylvania State University, University Park, PA 16802, USA
Received 2009 August 28; accepted 2009 September 23; published 2009 November 10

ABSTRACT

We present absolute parallaxes and relative proper motions for the central stars of the planetary nebulae NGC 6853 (The Dumbbell), NGC 7293 (The Helix), Abell 31, and DeHt 5. This paper details our reduction and analysis using DeHt 5 as an example. We obtain these planetary nebula nuclei (PNNi) parallaxes with astrometric data from Fine Guidance Sensors FGS 1r and FGS 3, white-light interferometers on the *Hubble Space Telescope*. Proper motions, spectral classifications and VJHKT$_2$M and DDO51 photometry of the stars comprising the astrometric reference frames provide spectrophotometric estimates of reference star absolute parallaxes. Introducing these into our model as observations with error, we determine absolute parallaxes for each PNN. Weighted averaging with previous independent parallax measurements yields an average parallax precision, $\sigma_\pi/\pi = 5\%$. Derived distances are: $d_{\rm NGC\,6853} = 405^{+28}_{-25}$ pc, $d_{\rm NGC\,7293} = 216^{+14}_{-12}$ pc, $d_{\rm Abell\,31} = 621^{+91}_{-70}$ pc, and $d_{\rm DeHt\,5} = 345^{+19}_{-17}$ pc. These PNNi distances are all smaller than previously derived from spectroscopic analyses of the central stars. To obtain absolute magnitudes from these distances requires estimates of interstellar extinction. We average extinction measurements culled from the literature, from reddening based on PNNi intrinsic colors derived from model SEDs, and an assumption that each PNN experiences the same rate of extinction as a function of distance as do the reference stars nearest (in angular separation) to each central star. We also apply Lutz–Kelker bias corrections. The absolute magnitudes and effective temperatures permit estimates of PNNi radii through both the Stefan–Boltzmann relation and Eddington fluxes. Comparing absolute magnitudes with post-AGB models provides mass estimates. Masses cluster around 0.57 $\mathcal{M}_\odot$, close to the peak of the white dwarf mass distribution. Adding a few more PNNi with well-determined distances and masses, we compare all the PNNi with cooler white dwarfs of similar mass, and confirm, as expected, that PNNi have larger radii than white dwarfs that have reached their final cooling tracks.

Key words: astrometry – planetary nebulae: general – stars: distances – stars: fundamental parameters – white dwarfs

Online-only material: color figures

1. INTRODUCTION

Planetary nebulae (PNe) are a visually spectacular and relatively short-lived step in the evolution from asymptotic giant branch (AGB) stars to a final white dwarf (WD) stage. Iben & Renzini (1983) first argued that the ejection of most of the gaseous envelope in AGB stars occurs during the thermal pulse phase, in the form of a massive, low-velocity wind. As summarized by Stanghellini et al. (2002), the remnant central star (PN nucleus, PNN; PN nuclei, PNNi) ionizes the gaseous ejecta, while a fast, low mass-loss rate PNN wind shapes the PN. PN morphology depends on a complicated combination of phenomena, some occurring within the nebular gas, which evolves on a dynamical timescale, and others caused by multiplicity and/or the evolution of the stellar progenitors and of the PNN. Morphology may also depend on the physical status of the interstellar environment of the PN progenitor.

Intercomparison of PNe can aid our understanding of the complicated astrophysics of this stage of stellar evolution, particularly if distances are known. Many indirect methods of PN distance determination exist (e.g., Ciardullo et al. 1999 and Napiwotzki 2001), including estimates from interstellar Na D lines, NLTE stellar atmospheres analyses of the PNNi (e.g., Hultzsch et al. 2007), estimates from resolved companion stars (Ciardullo et al. 1999), and from Galactic kinematics (Napiwotzki 2006). The expansion method (e.g., Palen et al. 2002) becomes model-dependent when applied to PNe with asymmetric or irregular geometry, and requires either an assumption that apparent expansion is due to material motions, or that one models the motion of the ionization front. Agreement among these distance determination methods is seldom better than 20%, often worse. Direct parallax measurements of PNNi rarely have precisions smaller than the measured parallax, a notable exception being Harris et al. (1997, 2007), who, using narrow-field CCD astrometry, provide ∼0.4 millisecond of arc (mas) precision parallaxes for PNNi nearer than ∼500 pc.

To further reduce the distance errors for a few PNNi (chosen as nearby from Harris et al. 1997), we have determined new absolute parallaxes of the PNNi of DeHt 5, Abell 31, and

* Based on observations made with the NASA/ESA *Hubble Space Telescope*, obtained at the Space Telescope Science Institute, which is operated by the Association of Universities for Research in Astronomy, Inc., under NASA contract NAS5-26555.

Table 1
PNNi Positions and Aliases

PN	R.A. (2000)	Decl.	Aliases		
NGC 6853	19 59 36.34	+22 43 16.1	Dumbbell	M 27	WD 1957+225
NGC 7293	22 29 38.55	−20 50 13.6	Helix	PN G036.1−57.1	WD 2226−210
DeHt 5	22 19 33.71	+70 56 03.3		PN G111.0+11.6	WD 2218+706
Abell 31	08 54 13.16	+08 53 53.0	PN A66 31	PK 219+31	PN CSI+09−08515

NGC 7293 (The Helix), using FGS 1r. Positions and aliases are given in Table 1. We have also determined a revised parallax for NGC 6853 (The Dumbell = M27) using previously collected FGS 3 data (Benedict et al. 2003) combined with several new FGS 1r measurements. Our present errors average 2–3 times smaller than those in Harris et al (2007). However, some reduction in the final parallax errors is obtained through a weighted average of our present parallaxes with those in Harris et al. (2007). Napiwotzki & Schoenberner (1995) classifies all the PNNi considered in this paper as WD of type DAO or DA.

Our reduction and analysis of these data is basically the same for our previous work on NGC 6853 (Benedict et al. 2003). Our extensive investigation of the astrometric reference stars provides an independent estimation of the line of sight extinction as a function of distance for these PNNi, a significant contributor to the uncertainty in the absolute magnitude, M_V. Using DeHt 5 as an example throughout, we present the results of extensive spectrophotometry of the astrometric reference stars, information required to derive absolute parallaxes from relative measurements; briefly discuss data acquisition and analysis; extract limits on binarity and photometric variability; and derive an absolute parallax for each PNNi. Finally, from a weighted average of our new parallaxes and those of Harris et al. (2007) we calculate an absolute magnitude for each PNN and derive stellar radii. With these and estimates of PNN mass from post-AGB evolution models we derive surface gravities, log g, to compare with those from the Napiwotzki (1999) stellar atmosphere analyses. We discuss some astrophysical consequences of these new, more precise distances and summarize our findings in Section 7.

Bradley et al. (1991) and Nelan (2007) provide an overview of the FGS instrument, and Benedict et al. (1999, 2002b, 2007) and Harrison et al. (2004) describe the fringe tracking (POS) mode astrometric capabilities of a Fine Guidance Sensor (FGS), along with the data acquisition and reduction strategies used in the present study. We time-tag all data with a modified Julian Date, mJD = JD − 2400000.5.

2. OBSERVATIONS AND DATA REDUCTION

Using DeHt 5 as an example, Figure 1 shows the distribution on the sky of the 10 reference stars and the PNN. This image is from the Digitized Sky Survey, via Aladin. For this target 15 sets of astrometric data were acquired with FGS 1r on the *Hubble Space Telescope* (*HST*), spanning 3.8 years, for a total of 248 measurements of the DeHt 5 PNN and reference stars. Each data set required approximately 33 minutes of spacecraft time. The data were reduced and calibrated as detailed in Benedict et al. (2002a, 2002b, 2007) and McArthur et al. (2001). At each epoch we measured reference stars and the target multiple times, this to correct for intra-orbit drift of the type seen in the cross filter calibration data shown in Figure 1 of Benedict et al. (2002b).

Table 2 lists the fifteen epochs of observation and highlights another particular difficulty with these data. Ideally (cf. Benedict et al. 2007), we obtain observations at each of the two maximum parallax factors[8] at two distinct spacecraft roll values imposed by the requirement that the *HST* roll to provide thermal control of the camera in the radial bay and to keep its solar panels fully illuminated throughout the year. This roll constraint generally imposes alternate orientations at each time of maximum positive or negative parallax factor over a typical two-year campaign. A few observations at intermediate or low parallax factors usually allow a clean separation of parallax and proper motion signatures. In the case of DeHt 5 (as well as Abell 31 and NGC 7293) two-gyro guiding[9] forced us into the less than satisfactory distribution of parallax factors shown in Table 2. Specifically for DeHt 5, there are no large positive parallax factors in right ascension. However, the higher the absolute declination of the target, the more likely it is that there will be windows of visibility near times of ±maximum parallax factor, either in R.A. or declination. Additionally, large declination typically results in higher ecliptic latitude. The ecliptic latitude of DeHt 5 renders its parallactic ellipse rather round, increasing the value of observations that were forced to be secured at times far from maximum parallax factor. We gain parallactic displacement in declination at the expense of displacement in R.A. These scheduling and solar-panel illumination constraints also resulted in the spotty access to our reference stars indicated in Table 2.

Finally, for DeHt 5 and Abell 31, we were able to take advantage of science instrument command and data handling (SIC&DH) computer problems that took the only other then operational science instrument (WFPC2) off-line in late 2008. This situation opened a floodgate of FGS proposals, temporarily rendering the *HST* nearly an "all astrometry, all the time" mission. Consequently, we obtained another epoch well-separated in time from the original eleven. This permitted a significantly better determination of relative proper motion for these two targets.

3. PNNI PHOTOMETRY AND COMPANION LIMITS

The FGS have two operating modes. We used both. The POS mode data collected over the course of this project can be used to establish the degree of photometric variability of these PNNi. Additionally, fringe scanning (TRANS mode) data provide an opportunity to discover previously unknown companions, or to establish limits for separation and magnitude difference.

3.1. FGS Photometry of the PNNi

FGS 1r and FGS 3 are precision photometers, yielding relative photometry with internal error $\gtrsim$ 0.002 mag (Benedict et al. 1998a). During each of the observation sets, we observed the PNNi 4–7 times over approximately 33 minutes. Given the

[8] Parallax factors are projections along R.A. and decl. of the Earth's orbit about the barycenter of the solar system, normalized to unity.

[9] The *HST* has a full compliment of six rate gyros, two per axis, that provide coarse pointing control. By the time these observations were in progress, three of the gyros had failed. The *HST* can point with only two. To "bank" a gyro in anticipation of a future failure, NASA decided to go to two gyro pointing as standard operating procedure.

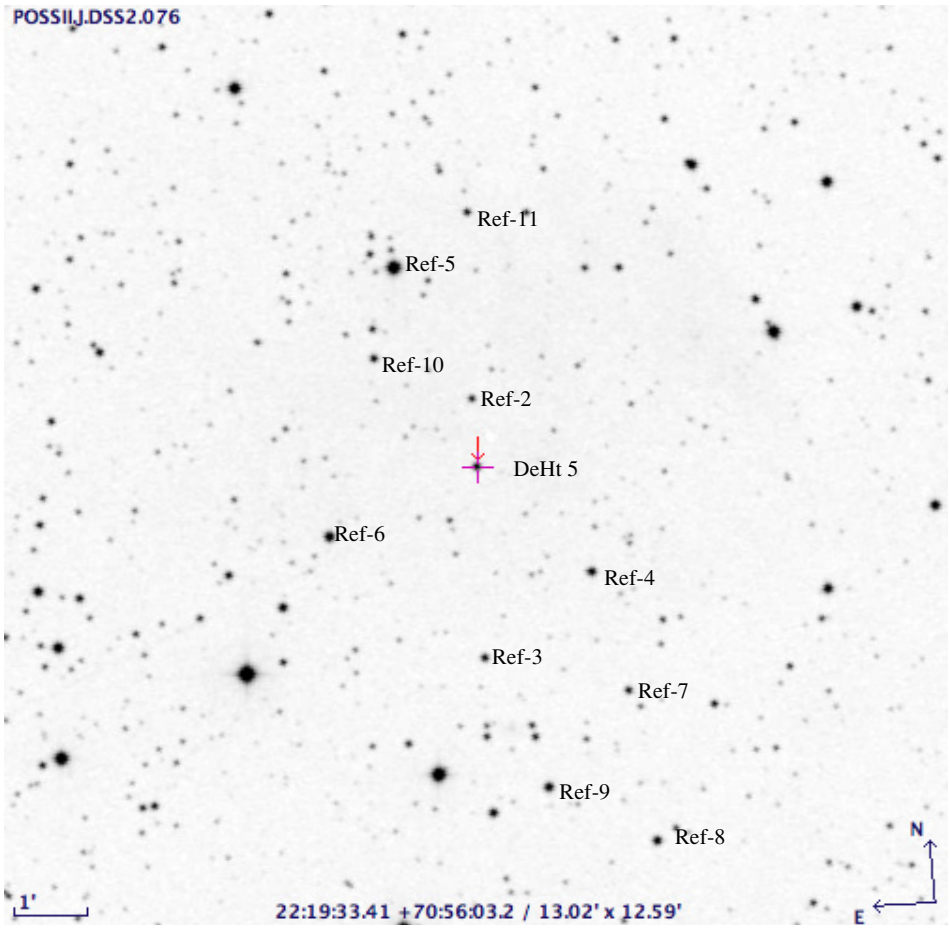

Figure 1. DeHt 5 central star and astrometric reference stars. Labels are immediately to the right of each star. (A color version of this figure is available in the online journal.)

Table 2
DeHt 5 Log of Observations and Reference Star Availability (x = Observed)

Set	mJD	P_α[a]	P_δ[b]	DeHt 5	2[c]	3	4	5	6	7	8	9	10	11
1	53390.0556	−0.5020	−0.8415	x	x	x	x	x		x	x	x	x	x
2	53392.0128	−0.4752	−0.8578	x	x	x	x	x		x	x	x	x	x
3	53587.7651	0.3155	0.9660	x	x	x	x	x		x	x	x	x	x
4	53587.8598	0.3147	0.9663	x	x	x	x	x		x	x	x	x	x
5	53623.0390	−0.2369	0.9536	x	x	x		x	x					
6	53671.1814	−0.8217	0.4197	x	x	x	x		x					
7	53764.2406	−0.3764	−0.9099	x	x	x	x	x		x	x	x	x	
8	53772.1216	−0.2563	−0.9501	x	x	x		x		x	x	x	x	x
9	53783.0153	−0.0818	−0.9759	x	x			x	x					
10	53956.0037	0.2697	0.9764	x	x	x	x	x	x					
11	53957.1156	0.2521	0.9805	x	x	x	x	x	x					
12	54780.6123	−0.8997	0.1901	x	x	x	x		x					
13	54780.6788	−0.9000	0.1890	x	x	x	x		x					
14	54780.7454	−0.9003	0.1879	x	x	x	x		x					
15	54782.5436	−0.9067	0.1574	x	x	x	x		x					

Notes.
[a] Parallax factor in right ascension.
[b] Parallax factor in declination.
[c] Reference star number.

faintness of these stars, we made no effort to explore for high-frequency variations during a single observation.[10] Standard deviations within any one observation set were on order 0.1% for the two brighter PNNi (NGC 6853 and NGC 7293), 0.2% for Abell 31, and 0.5% for DeHt 5. We derived a PNNi average intensity for each observation set and used the summed intensity of the brightest astrometric reference stars as a flat field. The resulting intensities were then transformed to relative magnitudes such that the average relative magnitude over the

[10] The FGS samples the fringe zero crossing at a 40 Hz rate. See Benedict et al. (1998b) for an example of the use of an FGS as a high-speed photometer, capturing a flare event in the vicinity of Proxima Cen.

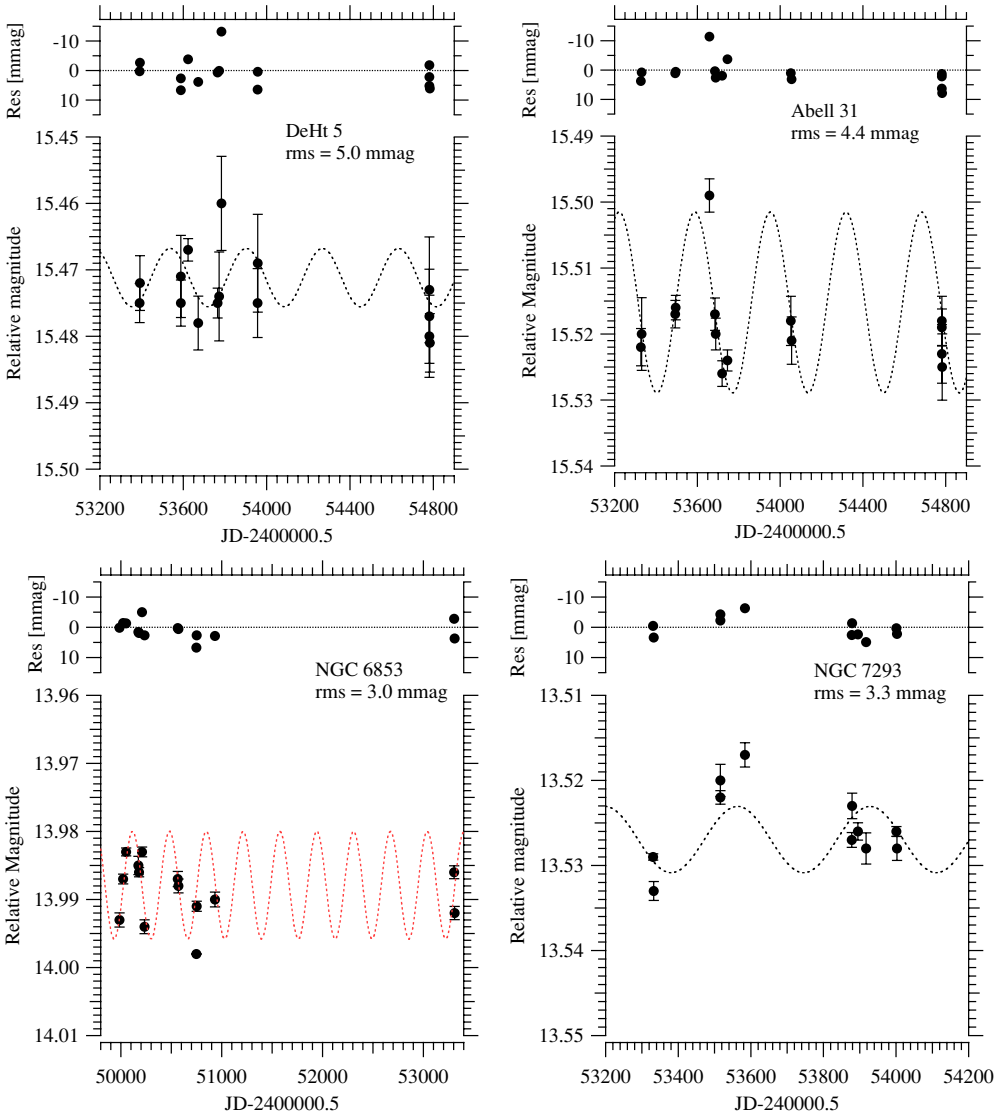

Figure 2. Photometric variations of the four PNNi observed with the FGS. In each panel the bottom section shows a fit to the original variation ascribed to roll-induced 1 yr period modulation of the stars used to generate each flat field. The top panel shows the residuals, each labeled with the final (presumed intrinsic) rms variation in the PNNi.

(A color version of this figure is available in the online journal.)

entire campaign matched the measured magnitude from Harris et al. (2007).

We show a montage of the resulting PNNi light curves in Figure 2. Our coverage is too sparse to extract any believable periodic astrophysical component to these variations. However, the internal errors for three PNNi suggest variations far larger than those expected from photometric errors only. This was expected. We fit these variations with sinusoids with periods of one year because of previously encountered position dependent variations of the brightnesses of the stars used to generate the flat field (see Benedict et al. 1998a, Section 2.3.1, for a discussion of roll-induced photometric variation). All PNNi were observed at similar positions within the FGS, typically with radial distances from pickle center $\leqslant 10''$. Variations introduced by Zodiacal light will be insignificant for the two brightest PNNi and for DeHt 5 at a high ecliptic latitude. Abell 31 is closest to the ecliptic, but nearly all observations were obtained at essentially identical Sun-target angular separations, resulting in little variation due to changing background. From Figure 2 and the statistics of intra-orbit observations, we conclude that an upper limit to photometric "flickering" on timescales of minutes to years is around 5 mmag.

3.2. Assessing PNNi Binarity

Companions of stellar and substellar mass have been invoked to produce the asymmetric structure seen in PN (Bond & Livio 1990; Soker 2006; De Marco 2009). Using FGS 1r TRANS mode observations (e.g., Franz et al. 1998, Nelan et al. 2004), we have analyzed the fringe morphology of these PNNi and find that all are unresolved. This places limits on separation and magnitude difference, Δm, for possible companions. Details on detectability can be found in Section 3.3.2 of the FGS Instrument Handbook (Nelan 2007). Summarizing the complex interplay among system magnitude, Δm, and separation, we would have detected companions with separations of 10 mas and larger with $\Delta m \leqslant 1$. Detectability at separations of 15 mas increases to $\Delta m \leqslant 2$. For separations $\geqslant 50$ mas, FGS 1r achieves a detectability of $\Delta m \leqslant 3.5$. Figure 3 compares the X and Y axis fringes of DeHt 5 with those from Abell 31.

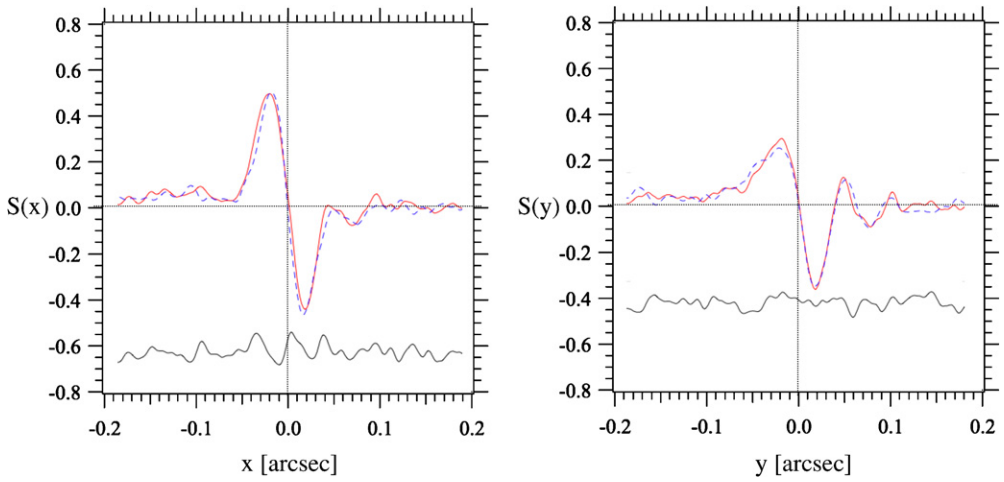

Figure 3. Fringes along *X* and *Y* axes of DeHt 5 (solid) and Abell 31 (dashed) compared. Residuals (bottom traces in each panel) indicate only the amplitude of noise expected for these relatively faint targets.

(A color version of this figure is available in the online journal.)

Either the two objects have identical companions, or they are both unresolved. Similar comparisons were made between NGC 6853 and NGC 7293 with similar results. Once we determine absolute magnitudes, parallaxes, and estimate masses for these PNNi, we will (Section 6.5.3) establish the spectral types, separations in AU, and periods for companions that would remain hidden from the FGS.

4. SPECTROPHOTOMETRIC ABSOLUTE PARALLAXES OF THE ASTROMETRIC REFERENCE STARS

Because the parallax determined for the PNNi will be measured with respect to reference frame stars that have their own parallaxes, we must either apply a statistically derived correction from relative to absolute parallax (Van Altena et al. 1995, hereafter YPC95) or estimate the absolute parallaxes of the reference frame stars listed in Table 2. In principle, the colors, spectral type, and luminosity class of a star can be used to estimate the absolute magnitude, M_V, and V-band absorption, A_V^*. The absolute parallax is then simply

$$\pi_{\rm abs} = 10^{-(V-M_V+5-A_V^*)/5}. \quad (1)$$

The luminosity class is generally more difficult to estimate than the spectral type (temperature class). However, the derived absolute magnitudes are critically dependent on the luminosity class. As a consequence, we obtained additional photometry in an attempt to confirm the luminosity classes. Specifically, we employ the technique used by Majewski et al. (2000) to discriminate between giants and dwarfs for stars later than $\sim$ G5, an approach also discussed by Paltoglou & Bell (1994).

4.1. Broadband Photometry

Our band passes for reference star photometry include: *BV* (CCD photometry from a 1 m telescope at New Mexico State University) and *JHK* (from 2MASS[11]). We also had access to Washington/DDO filters M, T_2, and DDO51 (obtained at Fan Mountain Observatory with the 1 m, and at Las Campanas Observatory with the Swope 1 m). Table 3 lists the visible and infrared photometry for the DeHt 5 reference stars, ref-2 through ref-11.

[11] The Two Micron All Sky Survey is a joint project of the University of Massachusetts and the Infrared Processing and Analysis Center/California Institute of Technology.

Table 3
DeHt 5 Astrometric Reference Star Photometry, Spectral Classifications, and Spectrophotometric Parallaxes

ID	V	$B-V$	$V-K$	SpT	M_V	A_V^*	$\pi_{\rm abs}$(mas)
Ref-2	15.56	0.82	2.29	F5 V	3.34	1.33	0.66 ± 0.15
Ref-3	14.90	0.82	2.2	F4 V	3.11	1.33	0.77 ± 0.19
Ref-4	14.31	0.96	2.54	G2 V	4.56	1.25	1.98 ± 0.46
Ref-5	11.92	0.48	1.24	F4 V	3.11	0.25	1.84 ± 0.45
Ref-6	13.55	0.6	1.63	F4 V	3.11	0.72	1.07 ± 0.26
Ref-7	15.02	1.06	2.76	G2 V	4.56	1.49	1.60 ± 0.37
Ref-8	14.90	0.83	2.72	F2 V	2.84	1.32	0.85 ± 0.17
Ref-9	13.50	1.42	3.75	K1 III	0.6	1.34	0.49 ± 0.12
Ref-10	14.94	0.92	2.52	F7 V	3.72	1.27	1.05 ± 0.24
Ref-11	14.86	1.48	3.88	K2 III	0.5	1.34	0.25 ± 0.06

4.2. Spectroscopy, Luminosity Class-sensitive Photometry, and Reduced Proper Motion

The spectra from which we estimated spectral type and luminosity class come from the New Mexico State University Apache Point Observatory.[12] The dispersion was 0.61 Å pixel^{-1} with wavelength coverage 4101–4905 Å, yielding $R \sim 3700$. Classifications used a combination of template matching and line ratios. The brightest targets had about 1500 counts above sky per pixel, or S/N $\sim$ 40, while the faintest targets had about 400 counts per pixel (S/N $\sim$ 20). The spectral types for the higher S/N stars are within $\pm$1 subclass. Classifications for the lower S/N stars are $\pm$2 subclasses. Table 3 lists the spectral types and luminosity classes for our reference stars.

The Washington/DDO photometry can provide a possible confirmation of the estimated luminosity class, depending on the spectral type and luminosity class of the star (later than G5 for dwarfs, later than G0 for giants). Washington/DDO photometry was more helpful as a discriminator for the DeHt 5 field than for our previous work on NGC 6853 (e.g., Benedict et al. 2003), suggesting a giant luminosity classification for ref-9 and ref-11. However, the problems related to the NGC 6853 PN nebulosity discussed in that paper also affected the NGC 7293 reference frame DDO photometry.

[12] The Apache Point Observatory 3.5 m telescope is owned and operated by the Astrophysical Research Consortium.

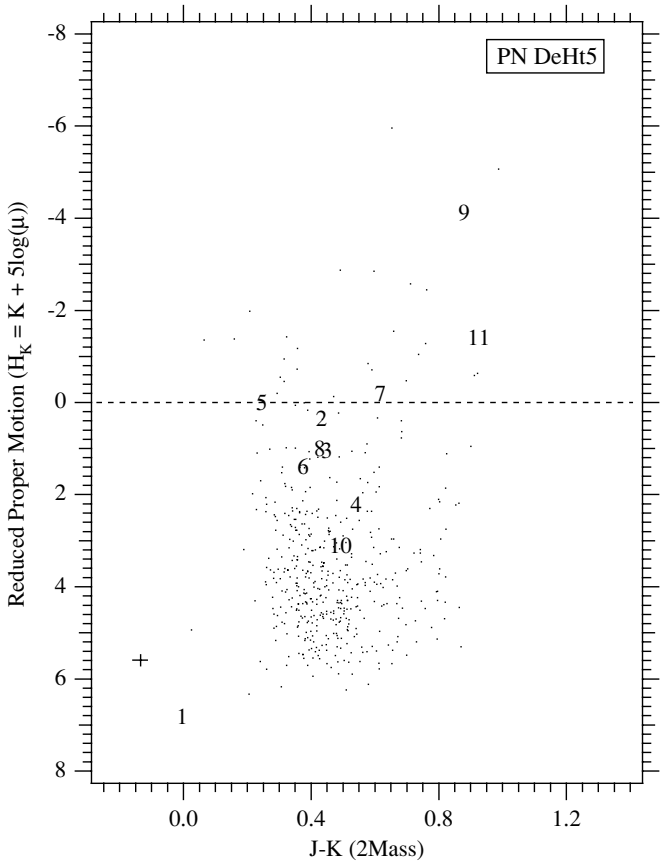

Figure 4. Reduced proper motion diagram for 458 stars in a 1° field centered on DeHt 5. Star identifications are shown for DeHt 5 (=1) and our astrometric reference stars. H_K for these stars is calculated using our final proper motions (Table 4). For a given spectral type giants and sub-giants have more negative H_K values and are redder than dwarfs in $J-K$. Reference stars ref-9 and ref-11 are confirmed to be giant stars. The cross in the lower left corner indicates representative errors along each axis.

We employ the technique of reduced proper motions to provide a confirmation of the reference star estimated luminosity class listed in Table 3. We obtain preliminary proper motions (μ) from UCAC2 (Zacharias et al. 2004) and J, K photometry from 2MASS for a one-degree-square field centered on DeHt 5. With final proper motions from our astrometric solution (Section 5.1) we plot Figure 4, which shows $H_K = K + 5\log(\mu)$ versus $(J-K)$ color index for 458 stars. If all stars had the same transverse velocities, Figure 4 would be equivalent to an H–R diagram. DeHt 5 and reference stars are plotted as ID numbers from Table 3. Errors in H_K are now ~0.3 mag. Reference stars 9 and 11 are clearly separated from the others, supporting their classification as giants.

4.3. Interstellar Extinction

To determine interstellar extinction, we first plot these stars on several color–color diagrams. A comparison of the relationships between spectral type and intrinsic color against those we measured provides an estimate of reddening. Figure 5 contains a $J-K$ versus $V-K$ color–color diagram and reddening vector for $A_V^* = 1.0$. Also plotted are mappings between spectral type and luminosity class V and III from Bessell & Brett (1988) and Cox (2000; hereafter AQ2000). Figure 5, and similar plots for the other measured colors, along with the estimated spectral types, provides an indication of the reddening for each reference star.

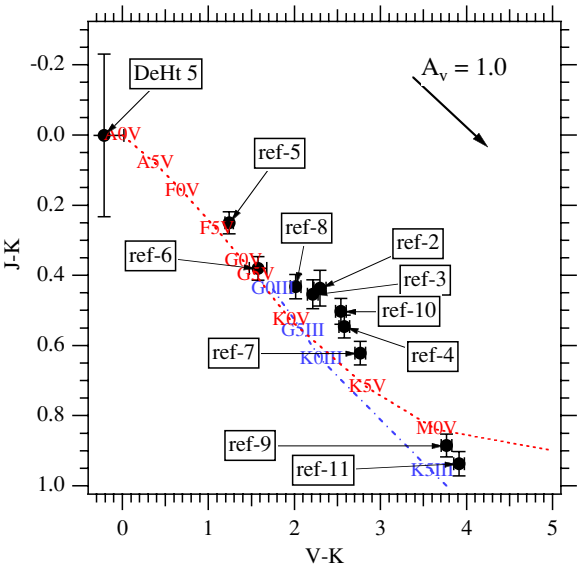

Figure 5. $J-K$ vs. $V-K$ color–color diagram. The dashed line is the locus of dwarf (luminosity class V) stars of various spectral types; the dot-dashed line is for giants (luminosity class III). The reddening vector indicates $A_V^* = 1.0$ for the plotted color system.

(A color version of this figure is available in the online journal.)

Assuming an $R = 3.1$ galactic reddening law (Savage & Mathis 1979), we derive A_V^* values by comparing the measured colors (Table 3) with intrinsic $B-V$, $J-K$, and $V-K$ colors from Bessell & Brett (1988) and AQ2000. Specifically we estimate A_V^* from three different ratios, each derived from the Savage & Mathis (1979) reddening law: $A_V^*/E(J-K) = 5.8$, $A_V^*/E(V-K) = 1.1$, and $A_V^*/E(B-V) = 3.1$. The resulting average A_V^* are collected in Table 3.

4.4. Adopted Reference Frame Absolute Parallaxes

We derive absolute parallaxes with M_V values from AQ2000 and the $\langle A_V^* \rangle$ derived from the photometry. Our parallax values are listed in Table 3. We produce errors on the absolute parallaxes by combining contributions from uncertainties in M_V and A_V^*, which we have combined and set to 0.5 mag for each reference star. Individually, no reference star parallax is better determined than $\frac{\sigma_\pi}{\pi} = 23\%$. The average absolute parallax for the DeHt 5 reference frame is $\langle \pi_{\rm abs} \rangle = 1.0$ mas. As a sanity check, we compare this to the correction to absolute parallax discussed and presented in YPC95 (Section 3.2, Figure 2). Entering YPC95, Figure 2, with the DeHt 5 galactic latitude, $l = -12°$, and average magnitude for the reference frame, $\langle V_{\rm ref} \rangle = 14.3$, we obtain a galactic model-dependent correction to absolute of 1.0 mas, in agreement.

5. ABSOLUTE PARALLAXES OF THE PN CENTRAL STARS

Sections 5.1–5.4 detail our astrometric modeling of the DeHt 5 data. Any differences in modeling for other PNNi are noted in Section 5.5. We compare our new distances with other more indirect estimates later in Section 6.5.4.

5.1. The DeHt 5 Astrometric Model

With the positions measured by FGS 1r, we determine the scale, rotation, and offset "plate constants" relative to an arbitrarily adopted constraint epoch (the so-called "master

plate") for each observation set (the data acquired at each epoch). The mJD of each observation set is listed in Table 2. The DeHt 5 reference frame contains 10 stars. We employ an eight-parameter model for those observations. For the DeHt 5 field, all the reference stars are redder than the science target. Hence, we also apply the corrections for lateral color discussed in Benedict et al. (1999).

As for all our previous astrometric analyses, we employ GaussFit (Jefferys et al. 1988) to minimize χ^2. The solved equations of condition for DeHt 5 are

$$x' = x + lc_x(B - V), \tag{2}$$

$$y' = y + lc_y(B - V), \tag{3}$$

$$\xi = Ax' + By' + C + R_x(x'^2 + y'^2) - \mu_x \Delta t - P_\alpha \pi_x, \tag{4}$$

$$\eta = Dx' + Ey' + F + R_y(x'^2 + y'^2) - \mu_y \Delta t - P_\delta \pi_y, \tag{5}$$

where x and y are the measured coordinates from *HST*; lc_x and lc_y are the lateral color corrections from Benedict et al. (1999); and $B - V$ are those colors for each star. A, B, D, and E are scale and rotation plate constants, C and F are offsets; R_x and R_y are radial term coefficients; μ_x and μ_y are proper motions; Δt is the epoch difference from the mean epoch; P_α and P_δ are parallax factors; and π_x and π_y are the parallaxes in x and y. We obtain the parallax factors (projections along R.A. and decl. of the Earth's orbit about the barycenter of the solar system normalized to unity) from a JPL Earth orbit predictor (Standish 1990), upgraded to version DE405.

5.2. Prior Knowledge and Modeling Constraints

In a quasi-Bayesian approach the reference star spectrophotometric absolute parallaxes (Table 3) and proper motion estimates for DeHt 5 (Harris et al. 2007) and for the reference stars from UCAC2 (Zacharias et al. 2004) were input as observations with associated errors, not as hardwired quantities known to infinite precision. Input proper motion values have typical errors of 4–6 mas yr^{-1} for each coordinate. The lateral color calibration and the $B - V$ color indices are also treated as observations with error. Orientation to the sky is obtained from ground-based astrometry from 2MASS with uncertainties in the field orientation $\pm 0\overset{\circ}{.}05$. This value, too, was made available as an observation with error. We essentially model a 3D volume of the space that contains our science target and reference stars, all at differing distances.

5.3. Assessing Reference Frame Residuals

The Optical Field Angle Distortion calibration (McArthur et al. 2002) reduces as-built *HST* and FGS 1r distortions with amplitude $\sim 1''$ to below 2 mas over much of the FGS 1r field of regard. From histograms of the reference star astrometric residuals (Figure 6), we conclude that we have obtained satisfactory correction in the region available at all *HST* rolls. The resulting reference frame "catalog" in ξ and η standard coordinates (Table 4) was determined with $\langle \sigma_\xi \rangle = 0.3$ mas and $\langle \sigma_\eta \rangle = 0.3$ mas. Relative proper motions along R.A. (x) and decl. (y) are also listed in Table 4. The proper motion vector is listed in Table 5, as are astrometric results for the other PNNi, including catalog statistics.

To determine if there might be unmodeled—but possibly correctable—systematic effects at the 1 mas level, we plotted

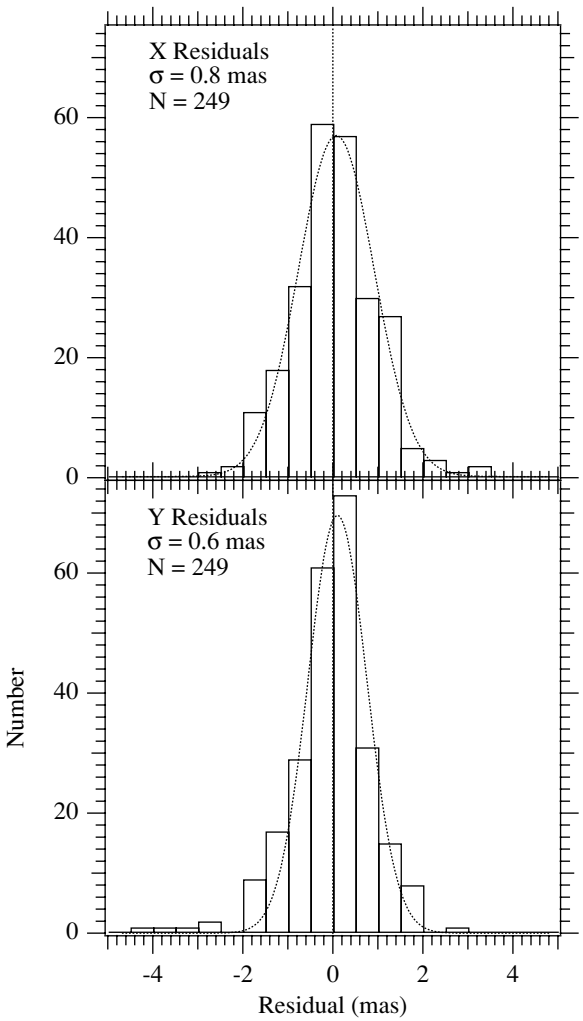

Figure 6. Histograms of x and y residuals obtained from modeling DeHt 5 and the astrometric reference stars with Equations (4) and (5). Distributions are fit with Gaussians whose σ's are noted in the plots.

the DeHt 5 reference frame x and y residuals against a number of spacecraft, instrumental, and astronomical parameters. These included (x, y) position within the pickle-shaped FGS field of regard; radial distance from the center of the FGS field of regard; reference star V magnitude and $B - V$ color; and epoch of observation. We saw no obvious trends, other than an expected increase in positional uncertainty with reference star magnitude.

5.4. The Absolute Parallax of the DeHt 5 Central Star

For this object at high ecliptic latitude (note the large parallax factors in both R.A. and decl. in Table 2) we can solve for the separate x and y components of the parallax. These were $\pi_x = 2.79 \pm 0.17$ mas and $\pi_y = 3.19 \pm 0.35$ mas. We obtain for the DeHt 5 PNN a final absolute parallax $\pi_{\rm abs} = 2.86 \pm 0.16$ mas. Our result agrees within the errors with the previous ground-based parallax measurement of the DeHt 5 PNN (Harris et al. 2007), $\pi_{\rm abs} = 3.34 \pm 0.56$ mas. Parallaxes from the *HST* and USNO and relative proper motion results from the *HST* are collected in Table 5. Even though both proper motion determinations are relative, using different sets of reference stars, the proper motion vector agrees with that determined by USNO (Harris et al. 2007). For the remainder of this paper we adopt as the absolute parallax of the DeHt 5

Table 4
DeHt 5 and Reference Star Astrometric Data

ID	ξ[a]	η[a]	μ_x[b]	μ_y[b]	π_{abs}[c]
DeHt 5[d]	−4.5797 ± 0.0001	−2.5814 ± 0.0001	−11.80 ± 0.10	−18.49 ± 0.08	2.86 ± 0.16
Ref-2	−3.5388 ± 0.0002	52.3476 ± 0.0001	−3.19 ± 0.11	−5.59 ± 0.10	0.70 ± 0.05
Ref-3	−2.0182 ± 0.0002	−156.6239 ± 0.0002	−2.51 ± 0.12	−5.21 ± 0.13	0.90 ± 0.03
Ref-4	−92.2348 ± 0.0003	−92.3332 ± 0.0002	1.73 ± 0.12	1.77 ± 0.16	1.30 ± 0.04
Ref-5	53.3040 ± 0.0001	161.1489 ± 0.0001	0.20 ± 0.24	−7.28 ± 0.28	1.50 ± 0.05
Ref-6	117.4994 ± 0.0002	−52.1638 ± 0.0002	2.15 ± 0.10	−4.14 ± 0.10	1.10 ± 0.08
Ref-7	−116.1855 ± 0.0004	−189.3931 ± 0.0004	6.41 ± 0.55	5.39 ± 0.64	0.80 ± 0.15
Ref-8	−132.3795 ± 0.0003	−311.4981 ± 0.0004	0.43 ± 0.50	0.10 ± 0.47	1.21 ± 0.10
Ref-9	−47.7228 ± 0.0003	−263.5350 ± 0.0003	−3.29 ± 0.50	−1.06 ± 0.49	0.34 ± 0.16
Ref-10	73.5099 ± 0.0004	89.0934 ± 0.0003	0.30 ± 0.41	1.17 ± 0.51	1.01 ± 0.08
Ref-11	−8.2819 ± 0.0006	202.4660 ± 0.0007	−1.16 ± 0.96	1.07 ± 1.02	0.21 ± 0.16

Notes.
[a] ξ (R.A.) and η (decl.) are relative positions in arcseconds.
[b] μ_x and μ_y are relative motions in mas yr^{-1}, where x and y are aligned with R.A. and decl.
[c] Absolute parallax in mas.
[d] R.A. = 22^{h}19^{m}33.^{s}713 + 70°56′03.″28, J2000, epoch = mJD 53764.24692.

Table 5
Reference Frame Statistics and PNNi Parallax and Proper Motion

Parameter	PNNi			
	DeHt 5	Abell 31	NGC 7293	NGC 6853
HST Study Duration (yr)	3.81	3.99	1.84	9.10
Observation Sets (#)	15	15	11	12
Ref stars (#)	10	6	3	7
Ref stars $\langle V \rangle$	14.29	13.56	13.11	14.37
Ref stars $\langle B-V \rangle$	0.94	0.80	0.69	1.28
$\langle \sigma_\xi \rangle$ (mas)	0.3	0.3	0.9	0.3
$\langle \sigma_\eta \rangle$ (mas)	0.3	0.2	0.9	0.3
HST π_{abs} (mas)	2.86 ± 0.16	1.51 ± 0.26	4.67 ± 0.33	2.22 ± 0.19
HST Relative μ (mas yr^{-1})	21.93 ± 0.12	10.49 ± 0.13	38.99 ± 0.24	8.70 ± 0.11
in Position Angle (°)	212.5 ± 0.10	227.1 ± 0.2	100.1 ± 0.3	67.9 ± 0.11
USNO Ref stars (#)	15	5	6	28
Ref stars (#) in common	3	0	1	2
USNO π_{abs} (mas)	3.34 ± 0.56	1.76 ± 0.33	4.56 ± 0.49	3.17 ± 0.32
USNO Relative μ (mas yr^{-1})	21.40 ± 0.20	10.40 ± 0.10	33.0 ± 0.1	13.50 ± 0.25
in Position Angle (°)	214.6 ± 0.5	226.5 ± 0.6	86.7 ± 0.3	60.8 ± 1.0
Weighted *HST*+USNO π_{abs}	2.90 ± 0.15	1.61 ± 0.21	4.64 ± 0.27	2.47 ± 0.16

PNN, $\pi_{abs} = 2.90 \pm 0.15$ mas, the weighted average of these two independent parallax determinations. The degree of independence is quantified in Table 5. Of the 10 reference stars used in the *HST* study, only three were in the suite of 15 (on average much fainter) reference stars used in the USNO study. If both studies used exactly the same set of reference stars, one would expect that some component of the uncertainties would be correlated. As indicated in Table 5, this is not the case for any of the PNNi investigated in our study.

5.5. Modeling Notes on the Other PNNi

Abell 31. This field provided six reference stars. The reference star average data are listed in Table 5. We again used the eight-parameter model (Equations (4) and (5)). Because of the low ecliptic latitude, most of the parallax signature is along R.A. Hence, we constrained $\pi_x = \pi_y$. Two gyro guiding scheduling constraints and the aforementioned science-side problems yielded a total study duration of four years. The *HST* parallax, $\pi_{abs} = 1.51 \pm 0.26$ mas, agreed well with the USNO value from Harris et al. (2007), $\pi_{abs} = 1.76 \pm 0.33$. For the remainder of this paper we adopt as the absolute parallax of the Abell 31 PNN, $\pi_{abs} = 1.61 \pm 0.21$ mas, the weighted average of these two independent parallax determinations. *HST*, USNO, and final *HST*+USNO weighted average parallaxes are given in Table 5. This distance, $d = 621^{+91}_{-70}$ pc, rules out a physical association between DeHt 5 and the red companion detected by the *HST* WFPC-2 camera discussed in Ciardullo et al. (1999).

NGC 7293. This field provided only three useful reference stars. The reference star average data are listed in Table 5. Because of the paucity of reference stars, the astrometric model for this field used only four parameters, discarding the radial terms and constraining $d = -b$, $e = a$ in Equations (4) and (5). We also constrained $\pi_x = \pi_y$. Model selection was dictated by the loss of access to 1–2 reference stars for many of the observation sets, primarily due to two-gyro guiding constraints on allowed spacecraft roll. One of the reference stars (#18 in the original GO-10432 proposal) was removed from our modeling. For several observation sets, each visit to that reference star locked on a different component. From these systematic residuals after initial modeling we inferred that it is either a binary or an optical double with component separation of ∼11 mas. Our NGC 7293 PNN parallax is $\pi_{abs} = 4.67 \pm 0.16$ mas.

van Leeuwen (2007) asserts that the intrinsic width of the main sequence for FGK stars is 0.4 mag (1σ). Past results

Table 6
PNNi Astrophysical Quantities

Parameter	PNNi			
	DeHt 5	Abell 31	NGC 7293	NGC 6853
V[a]	15.47	15.52	13.53	13.99
$B-V$[a]	−0.22	−0.29	−0.32	−0.30
d (pc)[b]	345^{+19}_{-17}	621^{+91}_{-70}	216^{+14}_{-12}	405^{+28}_{-25}
A^*_V	0.37 ± 0.07	0.10 ± 0.07	0.09 ± 0.04	0.30 ± 0.06
$m-M$	7.69 ± 0.12	8.97 ± 0.28	6.67 ± 0.13	8.04 ± 0.14
LKH Bias	−0.02 ± 0.02	−0.14 ± 0.03	−0.03 ± 0.01	−0.03 ± 0.01
M_V	7.39 ± 0.14	6.31 ± 0.30	6.74 ± 0.13	5.62 ± 0.16
$T^*_{\rm eff}$(K)[c]	76,500 ± 5,800	84,700 ± 4,700	103,600 ± 5,500	108,600 ± 6,800
BC	−5.84 ± 0.2	−6.29 ± 0.2	−6.77 ± 0.2	−6.91 ± 0.2
$M^*_{\rm bol}$	+1.55 ± 0.24	+0.03 ± 0.43	−0.03 ± 0.24	−1.29 ± 0.25
$H^{*\,d}_V$	1.12×10^8	1.24×10^8	1.62×10^8	1.72×10^8
$R_*(\odot)$	0.025 ± 0.002	0.039 ± 0.006	0.028 ± 0.003	0.045 ± 0.004
$\mathcal{M}_*(\odot)$[e]	0.57 ± 0.02	0.53 ± 0.03	0.60 ± 0.02	0.57 ± 0.01
log g[c]	6.7 ± 0.2	6.6 ± 0.3	7.0 ± 0.2	6.7 ± 0.2
log g[f]	7.41 ± 0.08	6.99 ± 0.14	7.34 ± 0.06	6.89 ± 0.08

Notes.
[a] From Harris et al. (2007).
[b] From weighted average of *HST* and Harris et al. (2007).
[c] From Napiwotzki (1999).
[d] erg cm^{-2} s^{-1} Å^{-1} str^{-1}.
[e] From Figure 9.
[f] From $g = \mathcal{M}G/R^2$.

(Benedict et al. 2007) indicate that for fields with 5 or more reference stars, cosmic dispersion in reference star absolute magnitude has no apparent consequence. In fact, Cepheid astrophysics argues that our parallax errors are overstated. To obtain a unity reduced χ^2 (χ^2 / dof, where dof = degrees of freedom) for our linear $M_V - \log P$ period–luminosity relation, we must significantly reduce our magnitude errors. For this one target whose parallax is dependent on only three reference stars we explored the effects of cosmic dispersion on reference star input absolute parallaxes. Worst-case (1σ increase or decrease in the M_V of all reference stars), the final absolute parallax for NGC 7293 could range ±0.29 mas. Hence we add in quadrature that error due to cosmic dispersion to our astrometry-only error for a final result of $\pi_{\rm abs} = 4.67 \pm 0.33$ mas. Harris et al. (2007) obtained $\pi_{\rm abs} = 4.56 \pm 0.49$ mas. A weighted average yields $\pi_{\rm abs} = 4.66 \pm 0.27$ mas. Our measured proper motion vector does not agree within the errors with the USNO value. This is not unexpected, given that our proper motion is measured against so few reference stars.

NGC 6853. As noted in Benedict et al. (2003) our original FGS 3-only data did not adequately cover the epochs of maximum parallax factor, resulting in a relatively (for the *HST*) poorly determined parallax, $\pi_{\rm abs} = 2.10 \pm 0.48$ mas. The addition of two new epochs of observation at maximum parallax factor with FGS 1r significantly increased the duration of the study (now over nine years) and improved the precision and slightly increased the parallax, now $\pi_{\rm abs} = 2.22 \pm 0.19$ mas. The astrometric model for this field used only six parameters, discarding the radial terms in Equations (4) and (5), a choice dictated by an insignificant decline in reduced χ^2 when increasing from 6 to 8 astrometric coefficients (Equations (4) and (5)). We also constrained $\pi_x = \pi_y$. For this object there are two USNO results (Harris et al. 1997, 2007) which yield the weighted USNO average $\pi_{\rm abs} = 3.17 \pm 0.32$ mas and the final *HST*+USNO weighted average $\pi_{\rm abs} = 2.47 \pm 0.16$ mas listed in Table 5. We note the significant difference in relative proper motion between the *HST* and USNO.

6. PNNi ABSOLUTE MAGNITUDES, RADII, AND MASSES

Again, we use DeHt 5 as an example of the steps required to obtain absolute magnitudes and radii for these PNNi. The final results for the other three PNNi are summarized in Table 6 and in individual notes (Section 6.4) below.

6.1. Absolute Magnitudes and the Lutz–Kelker–Hanson Bias

When using a trigonometric parallax to estimate the absolute magnitude of a star, a correction should be made for the Lutz–Kelker bias (Lutz & Kelker 1973) as modified by Hanson (1979). See Benedict et al. (2007), Section 5, for a more detailed rationale for the application of this correction to single stars. Because of the galactic latitude and distance of DeHt 5, and the scale height of the stellar population of which it is a member, we calculate Lutz–Kelker–Hanson (LKH) bias twice, assuming first a spheroidal then a disk distribution. The LKH bias is proportional to $(\sigma_\pi/\pi)^2$. Presuming that the PNN belongs to the same class of object as δ Cep (young, evolved main-sequence stars in a core helium burning phase), we scale the LKH correction determined for δ Cep in Benedict et al. (2002b) and obtain LKH = −0.02 mag. Presuming that the PNN belongs to the same class of object as RR Lyr (older, evolved main-sequence stars on the horizontal branch), we scale the LKH correction determined for RR Lyr in Benedict et al. (2002a) and obtain LKH = −0.03 mag. Our final LKH bias corrections are an average of the biases from the two adopted prior distributions. The corrections differ by at most 0.02 mag. See Benedict et al. (2007), Section 5, for a more

detailed rationale, justifying the use of this correction to single stars.

6.2. The Absolute Magnitude of the PNN of DeHt 5

Adopting for the DeHt 5 PNN $V = 15.47 \pm 0.03$ and the weighted average absolute parallax, $\pi_{\rm abs} = 2.90 \pm 0.15$ mas from Table 5, we determine a distance modulus, $m - M = 7.69 \pm 0.12$. To obtain a final absolute magnitude, we must correct for interstellar extinction. There are a variety of techniques used to estimate the extinction towards (and internal to) planetary nebulae. Perhaps the most common is the assumption that in nebular conditions, the ratio of Hα/Hβ = 2.86, and any deviation from this value is assigned to extinction. Alternatively, the observed radio flux can lead to a prediction of the flux in Hβ assuming an optically thin nebula with a temperature of 10^4 K. Either technique leads to a value for a logarithmic extinction at Hβ usually denoted by c, where $E(B-V) = 0.83c$ (Milne & Aller 1975). Other techniques include assuming a single value for the color for the PN central star, using interstellar absorption features seen in the optical or ultraviolet spectra, or simply using field stars along similar lines of sight.

For DeHt 5 two estimates of c (Pottasch 1996; Phillips 2005) list $E(B-V) = 0.0$. Harris et al. (2007) derive $E(B-V) = 0.18$, assuming $(B-V)_{\rm o} = -0.38$, yielding ($R = A_V^*/E(B-V) = 3.1$) $A_V^* = 0.56$. Estimating with field stars, from Table 3 (Section 4.3) we derive a per-star, per-unit 100 pc distance absorption, $\langle A_V^* \rangle/100$ pc. The average of the three stars nearest the central target (see Figure 1), ref-2, -4, and -6, is $\langle A_V^* \rangle/100$ pc $= 0.09 \pm 0.01$. With this per-unit 100 pc $\langle A_V^* \rangle$ and the distance to the DeHt 5 central star, $d = 345^{+19}_{-17}$ pc, we obtain a total absorption for the PNN, $A_V^* = 0.32 \pm 0.03$. We also estimate A_V^* using the measured temperature and a grid of synthetic spectra of hot, compact stars Rauch (2003). We calculate an intrinsic $(B-V)_{\rm o} = -0.36$. This yields $A_V^* = 0.42 \pm 0.07$, where the error is obtained through a 50,000 trial Monte Carlo process. Given the scatter in A_V^* from the various determinations, we choose to average the determination from synthetic spectra and the reference star values, yielding $A_V^* = 0.37 \pm 0.07$, deeming the c determination flawed for this faint an object. Including the LKH correction we obtain an absorption-corrected magnitude, $V_0 = 15.03$. The distance modulus and V_0 provide an absolute magnitude $M_V = 7.39^{+0.14}_{-0.14}$.

6.3. A Radius for the PNN of DeHt 5

We employ two methods to derive a radius, both differential in nature. The first method employs the Stefan–Boltzmann relation, the second filter-averaged Eddington fluxes.

To estimate a radius, R_*, for this star using the Stefan–Boltzmann relation we require a distance, an absolute magnitude, an effective temperature, $T_{\rm eff}^*$, and a bolometric correction (BC). These quantities then yield a radius via differential comparison with the Sun. Our parallax provides a distance, $d = 345^{+19}_{-17}$ pc and an absolute magnitude, $M_V = 7.39 \pm 0.14$. Napiwotzki (1999) has estimated $T_{\rm eff}^* = 76,500$ K $\pm$ 5800 K from model atmosphere fits to the Balmer Hδ and Hϵ absorption lines. We calculated BCs from our synthetic photometry, by comparing the integrated surface flux $\sigma T_{\rm eff}^4$ with the surface flux through the V band filter including the filter constant (or in other words computing the offset between $M_{\rm bol}$ and M_V of a star with arbitrary radius). We set the zero point by adopting the following values for the Sun: $M_{\rm bol}^\odot = 4.75$ and $M_V^\odot = -26.74$. For DeHt 5 we calculate BC $= -5.84 \pm 0.2$, where the error is dominated by the uncertainty in $T_{\rm eff}^*$.

We obtain a PNN bolometric luminosity $M_{\rm bol} = M_V + {\rm BC} = +1.55 \pm 0.24$. R_* follows from the expression

$$M_{\rm bol}^\odot - M_{\rm bol}^* = 10 \log (T_{\rm eff}^*/T_{\rm eff}^\odot) + 5 \log (R_*/R_\odot), \quad (6)$$

where we assume for the Sun $T_{\rm eff}^\odot = 5800$ K. We find $R_* = 0.026 \pm 0.007$ $R_\odot$. The sources of error for this radius are in the absolute magnitude (i.e., the parallax), the BC, and the $T_{\rm eff}^*$.

A second way to obtain R_* involves the V-band average Eddington flux, H_V, discussed in Bergeron et al. (1995) and Holberg & Bergeron (2006). The latter carried out a careful photometric calibration of DA white dwarfs with pure hydrogen atmospheres. However, radiative levitation in the hottest white dwarfs causes metals to be present in the atmospheres on a level roughly equivalent to solar abundances (Barstow et al. 2003). This has some impact on the spectral energy distribution (SED) causing redistribution of flux from the UV to longer wavelengths. To take this into account we computed synthetic photometry in the Johnson system from NLTE model spectra calculated with solar abundances of important elements up to the iron group (Rauch 2003). The photometry is linked to the Vega system as outlined by Holberg & Bergeron (2006). The overall effect of the metals is that $B-V$ colors for hot PNNi are bluer by $\approx$0.03 mag, and the flux level in the V band increases by typically 0.2 mag compared to pure hydrogen atmospheres.

Our synthetic photometry provides H_V^* as a function of temperature for solar-metallicity WD of various temperatures calibrated against Vega. We obtain H_V^* for $T_{\rm eff}^* = 76,500$ K. With $H_V^{\rm Vega}$, we can derive R_* from

$$R_*^2 = \left(H_V^{\rm Vega}/H_V^*\right) 10^{-0.4(M_V^* - M_V^{\rm Vega})}. \quad (7)$$

We obtain for DeHt 5 with $T_{\rm eff}^* = 76,500$ K, $M_V^* = 7.39$ from our parallax, and $M_V^{\rm Vega} = +0.026$ an $R_* = 0.025 \pm 0.002$ $R_\odot$, where the radius error is obtained through a 50,000 trial Monte Carlo process. Given that the approach relying directly on the BC and the approach utilizing H_V yield R_* values that agree, we will use for the remainder of this paper the lower error, $R_* = 0.025 \pm 0.002$ $R_\odot$. For the other three objects the radius from Stefan–Boltzmann will be calculated as a confirmation only. The higher error from Stefan–Boltzmann is due primarily to the significant contribution to the error budget from the BC uncertainty. The error on this radius cannot be further reduced by a weighted average of the results from the two approaches, because their errors are highly correlated, both having contributions from the uncertainties in $T_{\rm eff}^*$ and M_V^*.

6.4. Notes on the Radii of Other PNNi

All quantities required to estimate the radii for our other PNNi, as we did for DeHt 5, are gathered in Table 6, where we also list our derived radii.

Abell 31. Kaler (1983) estimates $c = 0.0 \pm 0.4$. We note that the line of sight total extinction estimated by Schlegel et al. (1998) is $E(B-V) = 0.064$. In this case we derive an average absorption per 100 pc for the four astrometric reference stars nearest in angular distance to the PNN of $A_V^* = 0.05 \pm 0.04$. From Rauch (2003) we calculate an intrinsic $(B-V)_{\rm o} = -0.36$. This yields $A_V^* = 0.24 \pm 0.07$. The average of these methods

yields $A_V^* = 0.10 \pm 0.07$, which we adopt. The distance modulus and V_0 provide an absolute magnitude $M_V = 6.31^{+0.29}_{-0.26}$, where we have included an LKH correction (-0.14 ± 0.03) and its uncertainty and the small uncertainty in A_V^* in quadrature.

Napiwotzki (1999) has estimated $T_{\rm eff}^* = 84{,}700$ K $\pm$ 4700 K. From our synthetic photometry we calculate a BC $= -6.29 \pm 0.2$. As in Section 6.3, we compare bolometric luminosities with the Sun and find $R_* = 0.041 \pm 0.017\ R_\odot$. We obtain H_V^* for $T_{\rm eff}^* = 84{,}700$ K, again from our synthetic photometry, which yields $R_* = 0.039 \pm 0.006\ R_\odot$.

NGC 7293. It has a reliably low value for the extinction. Kaler (1983) finds a value of $c = 0.04$. Milne & Aller (1975) derive $E(B-V) = 0.01$ from Hβ and radio. Bohlin et al. (1982) using IUE observations derives $E(B-V) = 0.012 +/- 0.03$. Harris et al. (2007) quotes $E(B-V) = 0.03$ from BVI photometry of the central star (assuming $(B-V)_{\rm o} = -0.38$), while Pottasch (1996) uses the same technique and gets $E(B-V) = 0.0$. The extinction maps of Burstein & Heiles (1982) and Schlegel et al. (1998) would estimate a reddening of $E(B-V) \sim 0.03$ mag, consistent with the Na I measurements for the central star (Mauron & Kendall 2004). If we translate the values for c to $E(B-V)$, and incorporate all of the other values we get a mean of $\langle E(B-V)\rangle = 0.027 \pm 0.022$. Consistent with this value, we derive an average absorption per 100 pc from the three astrometric reference stars nearest in angular distance to the PNN. With a per-unit 100 pc $\langle A_V^*\rangle = 0.02 \pm 0.02$ and the measured distance to the NGC 7293 central star, $d = 216 \pm 13$ pc, we obtain a total absorption for the PNN, $A_V^* = 0.04 \pm 0.03$. Again we adopt an average of the estimates, $A_V^* = 0.09 \pm 0.04$, yielding $M_V = 6.74 \pm 0.13$, where we have included an LKH correction (-0.03 ± 0.01) and its uncertainty and the small uncertainty in A_V^* in quadrature.

Napiwotzki (1999) has estimated $T_{\rm eff}^* = 103{,}600$ K $\pm$ 5500 K, which yields BC $= -6.77$. Comparing bolometric luminosities with the Sun we obtain $R_* = 0.028 \pm 0.007\ R_\odot$. We obtain H_V^* for $T_{\rm eff}^* = 103{,}600$ K from our synthetic photometry, which yields $R_* = 0.028 \pm 0.003\ R_\odot$.

NGC 6853. To estimate A_V^* Barker (1984) finds $c = 0.17$ and Kaler et al. (1976) find $c = 0.02$. Bohlin et al. (1982) estimate $E(B-V) = 0.06 +/- 0.03$ from IUE observations, while Pottasch (1996) gets $E(B-V) = 0.10$ and Harris et al. (2007) find $E(B-V) = 0.07$ from central star photometry. Ciardullo et al. (1999) obtain $c = 0.11$. The mean with error is then $\langle E(B-V)\rangle = 0.08 \pm 0.06$, or $\langle A_V^*\rangle = 0.26 \pm 0.17$. Given this uncertain $\langle A_V^*\rangle$, we derive an average absorption per 100 pc for the three stars nearest the central target, ref-4, -5, and -8. A finder chart can be found in Benedict et al. (2003). With a per-unit 100 pc $\langle A_V^*\rangle = 0.07 \pm 0.03$ from these three stars and the measured distance to the NGC 6853 central star, $d = 405^{+28}_{-25}$ pc, we obtain a total absorption for the PNN, $A_V^* = 0.28 \pm 0.06$. We adopt an average $A_V^* = 0.30 \pm 0.06$ and obtain $M_V = 5.62 \pm 0.16$, where we have included an LKH correction (-0.03 ± 0.01) and its uncertainty and the 0.06 mag uncertainty in A_V^* in quadrature.

Napiwotzki (1999) has estimated $T_{\rm eff}^* = 108{,}600$ K $\pm$ 6800 K for which we obtain BC $= -6.91 \pm 0.2$, where the error is dominated by the uncertainty in the temperature and the behavior of the BC at these high temperatures. Comparing bolometric luminosities with the Sun we find $R_* = 0.046 \pm 0.012\ R_\odot$. Comparing H_V with Vega we obtain H_V^* for $T_{\rm eff}^* = 108{,}600$ K listed in Table 6, which then yields $R_* = 0.045 \pm 0.004\ R_\odot$. Given that the two approaches yield R_* values that agree within their errors, we adopt $R_* = 0.045 \pm 0.004\ R_\odot$.

6.5. Astrophysical Consequences

6.5.1. Radii: PNNi Versus WDs

Our four parallaxes, along with measured temperatures and apparent luminosities have resulted in four newly estimated radii for PNNi that, according to theory, should eventually descend to a WD cooling track. Previous investigations have yielded precise temperatures and radii (and masses) for five WD in visual, spectroscopic, and eclipsing binaries. These results (Sirius B, Holberg et al. 1998; Procyon B, Girard et al. 2000; 40 Eri B, Shipman et al. 1997) are collected in Provencal et al. (2002). To these we add Feige 24 (Benedict et al. 2000), which has $\sigma_\pi/\pi = 2.7\%$, hence, a reasonably well-determined radius, two PNNi from Harris et al. (2007), Sh 2-216 and HDW 4, both with $\sigma_\pi/\pi \leqslant 8\%$, and the eclipsing Hyades WD binary, V471 Tau (O'Brien et al. 2001). We will now compare PNNi and WD, using the quantities gathered in Table 7. We can also test the accuracy of the parallax and the many corrections leading to the bolometric magnitudes required by Equation (6), relating temperature, bolometric magnitude and radius. This aggregate of data probes the transition from PNNi to WD.

Let us for the moment assume that all PNNi have the same mass and radius. In such a universe the only PNNi and/or WD variable is age, hence, temperature, and there should be a relationship between absolute bolometric magnitude and temperature, through Stefan–Boltzmann, $L = 4\pi R^2 \sigma T^4$. Figure 7 (basically an H–R diagram) indicates that temperature and absolute bolometric magnitude are correlated, in that hotter PNNi and WD have brighter absolute magnitudes. This is not surprising, given that the measured or estimated mass of most of these objects lie in the range $0.44 < \mathcal{M}_\odot < 0.60$. For the WD, bolometric magnitudes are derived using BC from Flower (1996) and Bergeron et al. (1995). The most discrepant object is Sirius B, which has the greatest mass, $\mathcal{M}^* = 1.02\ \mathcal{M}_\odot$, hence, the smallest WD radius. If Equation (6) perfectly describes both PNNi and WD, then the residuals, $\Delta M_{\rm bol}$, in Figure 7 to our simple linear relationship between $M_{\rm bol}$ and $\log T$ should correlate with the log of the radius. Figure 8, wherein $\Delta M_{\rm bol}$ is plotted against log radius, shows such a correlation. The residuals in Figure 8 have an rms dispersion of 0.12 mag, indicating the accuracy of the LKH and extinction corrections. The two most discrepant objects are Feige 24 and Sirius B with residuals of order 0.2 mag.

6.5.2. PNNi Masses and Gravities

Various investigators have modeled the evolution of a star as it passes through the red giant phase, ejects significant mass, and becomes a white dwarf. The PN phase lies between the giant and WD stages in stellar evolution. To estimate PNNi mass we compare in Figure 9 the positions of our PNNi in an H–R diagram ($M_V - \log T_{\rm eff}$) with predicted evolutionary tracks of post-AGB stars from Schönberner & Blöcker (1996). Also plotted are tracks of lower mass stars from Driebe et al. (1999). Absolute V-band magnitudes, M_V, for tracks were calculated for solar metallicity, using SEDs from Rauch (2003). PNNi temperatures are from Napiwotzki (1999). We find that the four PNNi clump about a mass $\mathcal{M} = 0.57\ \mathcal{M}_\odot$, in agreement with the peak of the WD mass distribution, $0.60\ \mathcal{M}_\odot$, found by (Liebert et al. 2005). Interpolated individual masses are found in Table 6. We also estimate masses for PNNi

Table 7
Comparing PNNi and WD

ID	V_0	$(m-M)_0$	M_V[f]	BC	M_{bol}	log T (K)	log $R^*(\odot)$	$M(\odot)$[g]
DeHt 5[a]	15.15	7.69	7.39	−5.95	1.44 ± 0.28	4.884 ± 0.04	−1.61 ± 0.03	0.57 ± 0.02
Abell 31[a]	15.47	8.97	6.25	−6.3	−0.06 0.43	4.928 0.03	−1.40 0.06	0.53 0.03
NGC 7293[a]	13.50	6.67	6.74	−6.77	−0.03 0.24	5.015 0.03	−1.56 0.06	0.60 0.02
NGC 6853[a]	13.75	8.04	5.62	−7.09	−1.47 0.25	5.036 0.03	−1.35 0.04	0.57 0.01
Sh 2-216[b]	12.38	5.54	6.82	−6.30	+0.52 0.23	4.920 0.03	−1.47 0.10	0.55 0.03
HDW 4[b]	16.11	6.60	9.45	−4.47	4.98 0.28	4.674 0.03	−1.87 0.12	0.77 0.07
Feige 24[c]	12.56	4.17	8.39	−4.82	3.57 0.13	4.751 0.02	−1.73 0.02	0.57 0.02
V471 Tau[d]	13.72	3.39	10.33	−3.49	6.84 0.03	4.538 0.01	−1.97 0.01	0.84 0.05
Procyon B[e]	10.82	−2.28	13.1	0	13.1 0.03	3.889 0.01	−1.91 0.01	0.55 0.02
Sirius B[e]	8.44	−2.89	11.33	−2.3	9.03 0.1	4.394 0.01	−2.06 0.01[h]	1.02 0.02
40 Eri B[e]	9.5	−1.49	10.99	−1.5	9.49 0.1	4.223 0.01	−1.87 0.006	0.501 0.011

Notes.
[a] From this paper.
[b] From Harris et al. (2007).
[c] From Benedict et al. (2000).
[d] From O'Brien et al. (2001). BC from Flower (1996) and Bergeron et al. (1995).
[e] From compilation of Provencal et al. (2002). BC from Flower (1996) and Bergeron et al. (1995).
[f] Includes LKH bias correction, negligible for the last four objects.
[g] From this paper and Provencal et al. (2002), except Feige 24 from Kawka et al. (2008), Procyon B and Sirius B from Schaefer et al. (2006) and Bond (2009).
[h] From Barstow et al. (2005).

HDW 4 and Sh2-216. These are listed in Table 7. We note that the mass of 40 Eri B from these tracks is $\sim 0.9\,\mathcal{M}_\odot$, differing substantially from that listed in Provencal et al. (1998).

A mass and radius uniquely determine a surface gravity, g, through

$$g = MG/R^2, \tag{8}$$

where G is the gravitational constant. Our DeHt 5 radius, $R_* = 0.025 \pm 0.002\,R_\odot$ and the mass inferred from the evolutionary tracks in Figure 10 (where we plot radius versus $T_{\rm eff}$), $\mathcal{M} = 0.57 \pm 0.02\ \mathcal{M}_\odot$, yield $\log g = 7.41 \pm 0.08$. The uncertainty in our $\log g$ is primarily due to the radius uncertainty. For Abell 31 our mass estimate, $\mathcal{M} = 0.53 \pm 0.03\ \mathcal{M}_\odot$ with our radius determines a gravity, $\log g = 6.96 \pm 0.14$. For NGC 7293 using the radius from the H_V^* approach and a mass estimated from Figure 9, $\mathcal{M} = 0.60 \pm 0.02\ \mathcal{M}_\odot$ determines a gravity, $\log g = 7.34 \pm 0.06$. For NGC 6853 our mass estimate, $\mathcal{M} = 0.57 \pm 0.01\ \mathcal{M}_\odot$ with our radius determines a gravity, $\log g = 6.89 \pm 0.08$, in agreement with the Napiwotzki (1999) line profile fitting value, $\log g = 6.7 \pm 0.2$. Calculated values of $\log g$ for our four PNNi are listed in Table 6 and compared with the Napiwotzki (1999) line profile fitting values. Note that Figure 10 shows 40 Eri B to have a mass consistent with past estimates. In Figure 11 we compare our WD sample with the PNNi listed in Table 7 on a mass–radius diagram. Most of the PNNi and the hottest WD, Feige 24, lie above the zero-temperature mass–radius relationship from Hamada & Salpeter (1961). These radii confirm that PNNi are larger than cooler WD.

6.5.3. Limits on Stellar Companions

With the parallaxes from Table 5, absolute magnitudes and mass estimates from Table 6, and the separation and Δm detection limits from Section 3.2, we can now estimate the spectral type, separation in AU and periods for companions at the limit of detectability. Companions with spectral types later than listed in Table 8 would not be detected by the FGS. For example, a companion 2 mag fainter than the DeHt 5 PNN (an

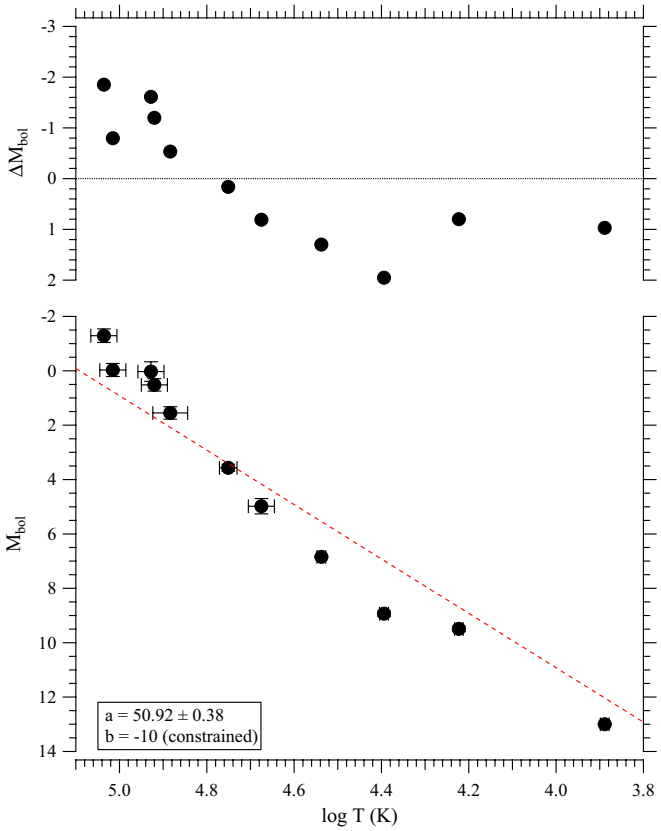

Figure 7. Absolute bolometric magnitude, $M_{\rm bol}$, plotted against log temperature. The slope is constrained to the theoretical value. $M_{\rm bol}$ for the PNNi comes from our parallax, the apparent magnitude, the BC, and the interstellar absorption, A_V^* (Table 6) and Harris et al. (2007). The WD values are from Benedict et al. (2000) for Feige 24, from O'Brien et al. (2001) for V471 Tau, and calculated from Provencal et al. (2002), with BC from Flower (1996) and Bergeron et al. (1995) for Sirius B, 40 Eri B, and Procyon B. All relevant quantities are collected in Table 7. With much scatter the PNNi and WD appear to exhibit an approximate absolute bolometric magnitude–temperature relation, one that would hold, assuming similar radii and masses for all PNNi and WD. Both Equation (6) and the residuals, $\Delta M_{\rm bol}$, argue otherwise.

(A color version of this figure is available in the online journal.)

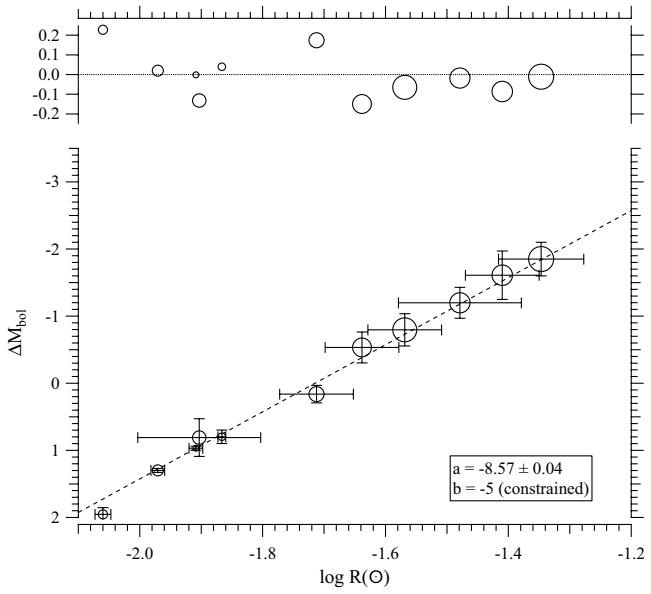

Figure 8. Residuals, $\Delta M_{\rm bol}$, from the linear $M_{\rm bol}-\log T$ relationship for PNNi and WDs in Figure 7 plotted against the logarithm of the radius in solar units. The slope is constrained to the value expected from Equation (6). The symbol size is proportional to surface temperature. The expected linear residual correlation (- - -) with log R exhibits an rms scatter of 0.12 mag.

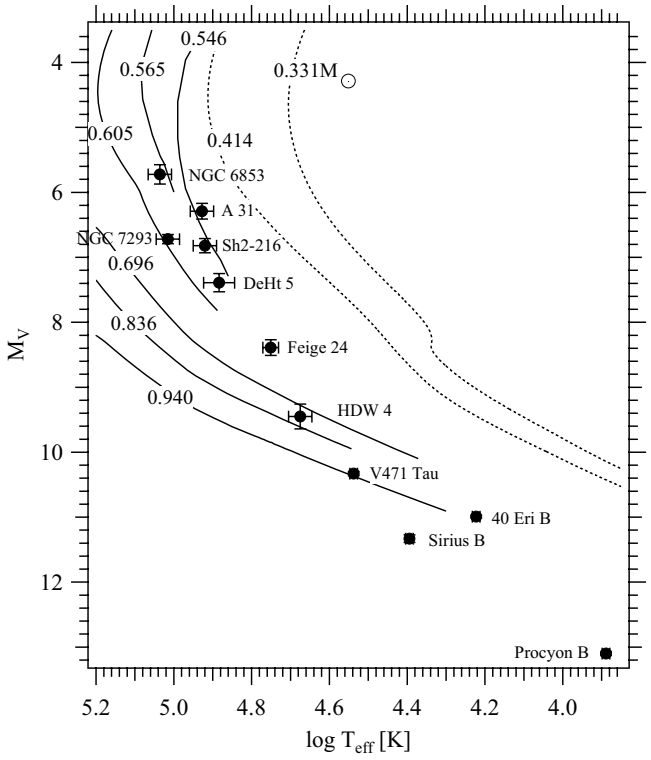

Figure 9. PNNi and WD absolute magnitude, M_V, plotted against log temperature. M_V for the PNNi comes from our parallax, the apparent magnitude, and the interstellar absorption, A_V^* (Table 6) with two additional (HDW 4, Sh2-216) from Harris et al. (2007). The WD values are from Benedict et al. (2000) for Feige 24, from O'Brien et al. (2001) for V471 Tau, and calculated from Provencal et al. (2002). All relevant quantities are collected in Table 7. The higher-mass (solid line) evolutionary tracks are from Schönberner & Blöcker (1996). Lower-mass (dashed line) tracks are from Driebe et al. (1999). The PNNi clump around $M = 0.57\ M_\odot$.

M1V star) is at the limit of detectability for a separation of 15 mas, which for the parallax of DeHt 5 equates to 5.2 AU. From $P^2(M_1 + M_2) = a^3$ we derive a period $P = 11$y. For

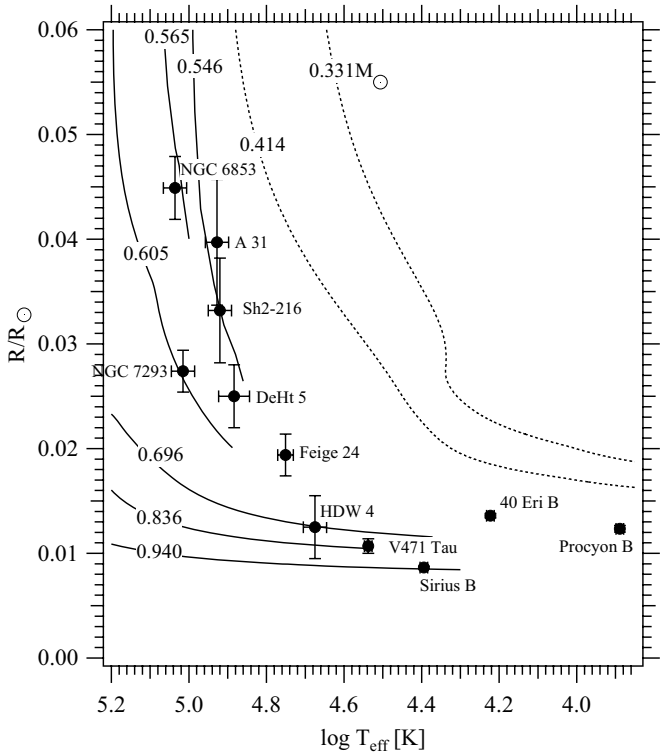

Figure 10. PNNi and WD radii from Table 7 plotted against log temperature. The evolutionary tracks for objects of high and low masses are from Schönberner & Blöcker (1996) and Driebe et al. (1999). In this mapping the WD Procyon B and 40 Eri B appear to have masses consistent with previous measurements.

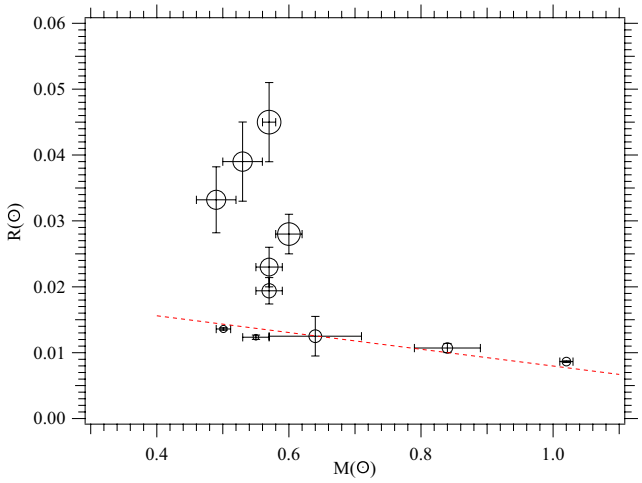

Figure 11. Mass–radius diagram for six PNNi and five WDs with precise radii and masses (Table 7). From top to bottom we plot NGC 6853, Abell 31, Sh2-216, NGC 7293, DeHt 5, Feige 24, 40 Eri B, HDW 4, Procyon B, V471 Tau, and Sirius B. Symbol size is proportional to surface temperature. The dashed line is the Hamada & Salpeter (1961) carbon core relationship. Except for the coolest PNN, HDW 4, the PNNi (and the hottest WD, Feige 24) have larger radii than the cooler WD.

(A color version of this figure is available in the online journal.)

another application of Table 8 we consider NGC 7293. Su et al. (2007) find evidence for IR-emitting dust 35–150 AU from the PNN of NGC 7293. A binary companion could provide an engine to sculpt a dust disk. Given that 35 AU at the distance of NGC 7293 is 0.″16 and that we would detect a companion with $\Delta m \leqslant 3.5$, that companion would have to have a spectral type later than M1 V. If much asymmetrical PN structure is due to binarity (Soker 2006; De Marco 2009), then we would have the highest probability of detecting the companion to the PNN of

Table 8
Companion Limits from FGS Fringe Scanning

ID	M_V	π_{abs}	$\mathcal{M}_*(\odot)$	ΔV	Comp 2 SpT	Comp 2 $\mathcal{M}(\odot)$	Sep (AU)	P (yr)
DeHt 5	7.39	2.9	0.57	1	K8V	0.59	3.4	6
				2	M1V	0.53	5.2	11
				3	M2V	0.4	17.2	73
Abell 31	6.23	1.61	0.53	1	K4V	0.7	6.2	14
				2	K8V	0.59	9.3	27
				3	M1V	0.53	31.1	168
NGC 7293	6.77	4.66	0.6	1	K6V	0.64	2.1	3
				2	M0V	0.51	3.2	5
				3	M1V	0.53	10.7	33
NGC 6853	5.62	2.47	0.57	1	K3V	0.72	4.0	7
				2	K6V	0.64	6.1	14
				3	M0V	0.51	20.2	88

NGC 6853, the most asymmetric of the PN we observed. Our null detection suggests that such a companion is likely to have $P < 7$y and $\mathcal{M} < 0.7\ \mathcal{M}_\odot$.

Finally, in principle we can probe for very short period companions using the photometry in Figure 2. Companions with small separations could produce a single-peaked orbital light curve through heating of the companion star by the PNN e.g., the reflection effect. As the companion star orbits the PNN, its heated face is alternately more or less visible, increasing and decreasing the observed flux from the PNN once per orbit. For example, the Feige 24 system (WD+M2 V) has a period of $4\overset{d}{.}23$ and from FGS photometry (Benedict et al. 2000) evidences a photometric variation of 25 mmag. Kawka et al. (2008) estimate an inclination $i = 77°$. Assuming a similar inclination, we find from binary light curve modeling (cf. Harrison et al. 2009) that even the shortest period companions would produce less V band variation from reflection effects than we see in Figure 2. PNNi are too bright, washing out any variations due to reflection from companions.

6.5.4. Comparison with other Distance Estimates

Napiwotzki (2001) has compiled PNe distances from a number of methods. Figure 12 plots our distances from Table 6 against three other methods: distances obtained via non-LTE PNNi atmosphere analysis (Napiwotzki 2001), from an Hβ-diameter relation devised by Shklovski (1956), and from an interstellar Na D line analysis (Napiwotzki & Schoenberner 1995). Shklovski distances are only available for only three of our targets, and the Na D method has been applied only to two of our targets. The recent recalibration of the Shklovski distances by Stanghellini et al. (2008) left those three distances basically unchanged. The dashed line represents perfect agreement. The Shklovski approach has a tendency to underestimate the distances while the spectroscopic distances are a bit on the high side. We now provide a more detailed assessment of distances obtained via non-LTE PNNi atmosphere analysis.

6.5.5. Reassessing the Spectroscopic Distance Scale for PNNi

Napiwotzki (1999) determined PNNi fundamental stellar parameters, temperature and surface gravity, from a fit of the hydrogen Balmer lines with profiles computed from NLTE model atmospheres. This technique is well established and tested for the analysis of hot white dwarfs (e.g., Finley et al. 1997) using LTE atmospheres. However, when Napiwotzki (1999) applied this method to the even hotter central stars of

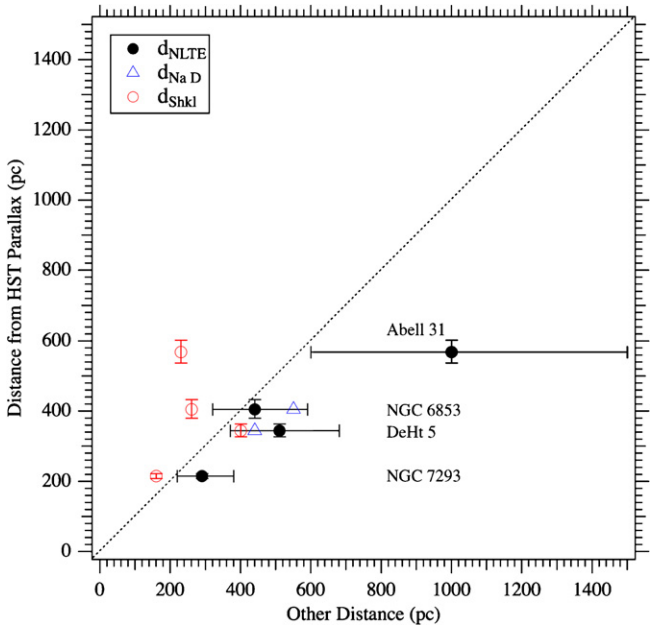

Figure 12. Distances from weighted averages of *HST* (this paper) and USNO (Harris et al. 2007) parallaxes compared to distances from NLTE analysis ("•", Napiwotzki 2001), Hβ-derived distances from ("○", Shklovski 1956), and distances estimated from interstellar Na D ("△", Napiwotzki & Schönberner 1995). The dashed line represents perfect agreement. Objects are labeled to the right or top.

(A color version of this figure is available in the online journal.)

old PNe, it became clear that for many stars no consistent fit of all Balmer lines could be achieved. A strong temperature trend was present, with the fit of higher members of the Balmer series yielding higher temperatures. This became known as the Balmer line problem (Napiwotzki & Rauch 1994).

Napiwotzki (1993, 1999) presented arguments that the temperature derived from the highest Balmer lines Hδ and Hϵ are close to the real temperatures of the PNNi. However, a physical explanation of the Balmer line problem remained elusive for some time. Models used for the Napiwotzki (1999) investigation were calculated in full NLTE but included only the two most abundant elements hydrogen and helium. Tests carried out prior to the start of this project appeared to show that the impact of line blanketing of heavier elements on the temperature structure of the atmospheres had only minor impact on the hydrogen line profiles (see discussion in Werner 1996). However, Werner (1996) could show that strong cooling by the resonance

lines of carbon, nitrogen, and oxygen can reproduce the observed Balmer lines in the hot sdO BD+28°4211 and the PNN of Sh 2–216, if detailed treatment of the Stark broadening of these lines is included in the calculations. This treatment is very computer time intensive. For this reason, it was not included in previous calculations. The Werner (1996) results provided an astrophysical explanation and essentially validated the recipe of adopting the temperature fitted for Hδ and Hϵ put forward in Napiwotzki (1993). This method was then adapted by Napiwotzki (1999).

Fitted surface gravities appeared to be unaffected by the Balmer line problem. All Balmer lines could be fitted with a single value of g using the Napiwotzki (1999) H and He models. Also, the Werner (1996) calculations did not indicate offsets in gravity. Napiwotzki (2001) compared his spectroscopic distance estimates with the results of other distance estimates including the best parallax measurements available at that time (Harris et al. 1997). The comparison showed spectroscopic distances larger than trigonometric distances by 55%—at face value. However, as pointed out by Napiwotzki (2001), one has to take into account that the often significant relative errors of trigonometric parallaxes introduce sample biases. Lutz–Kelker biases are one way to estimate the size of the effect. Napiwotzki (2001) performed a Monte Carlo simulation trying to model the properties of the Harris et al. (1997) sample as closely as possible given the—by necessity—not well defined selection criteria. The result was an estimated bias of the trigonometric distances, now too small by 32% $\pm$ 0.25%. The conclusion at that time was that both distance scales are marginally consistent, but large uncertainties remained.

Improved accuracy of recent trigonometric parallax measurements have changed the situation dramatically. Harris et al. (2007) achieved accuracies ranging from 0.3 mas to 0.6 mas. The measurements presented in our investigation yield even better accuracies with σ_π being 0.21 mas and below. Harris et al. (2007) estimates a bias of 5% for their sample. A straightforward reading from Table A.2 in Napiwotzki (2001) gives an estimate of 7% for a sample with 0.2 mas accuracy. Both estimates confirm that remaining systematic errors are now much smaller, in line with the small Lutz–Kelker biases given in our Table 6. Thus it is a good time to reassess the spectroscopic distance scale.

Spectroscopic distances of the four program stars are 38% larger than the trigonometric distances (unweighted average). This offset is smaller than that found by Napiwotzki (2001), but due to the smaller errors and biases it is now highly significant. This translates into an average $\log g$ offset $\overline{\log g_{\rm spec} - \log g_\pi} = -0.41$. In Table 6 we find DeHt 5 anomalous, the difference between gravity derived from our radius and from the analysis of stellar atmospheres larger than for the other three PNNi. DeHt 5 is of special interest and will be discussed below. Excluding DeHt 5 from the average we compute an average distance offset of 40% (spectroscopic distances recomputed using the improved photometric observations, reddening estimates and synthetic photometry) and $\log g$ offset of 0.30, not much larger than typical gravity errors given in Napiwotzki (1999) which are 0.2–0.3 dex.

6.5.6. The Case of DeHt 5

The temperature and gravity derived by Napiwotzki (1999) place the central star of DeHt 5 in a region of the temperature gravity diagram inconsistent with a post-AGB origin. The parameters of this central star were better matched to those of a star that lost its envelope at the end of the first red giant branch and is now evolving into a low mass He-core white dwarf. Barstow et al. (2001) performed an analysis of optical and UV spectra using model atmospheres including the effect of model line blanketing. The derived temperature is 57,400 K—lower than the Napiwotzki (1999) result—partly due to the inclusion of metal line blanketing and partly due to a different fit algorithm and philosophy. The gravity $\log g = 7.0$ given by Barstow et al. (2001) is essentially an upper limit, because it was the lowest $\log g$ available in the model atmosphere grid. The gravity resulting from a fit with pure hydrogen models is in good agreement with the Napiwotzki (1999) result: $\log g = 6.75$ versus 6.65.

None of the results can be reconciled with the trigonometric results, which translates into $\log g = 7.4$. Barstow et al. (2001) also determined metal abundances from the analysis of an *HST*–STIS UV spectrum. The resulting abundances are higher than those of the well-known hot "template" white dwarf G 191–B2B, which appears to have typical abundances for that parameter range (Barstow et al. 2003). One could be tempted to speculate that unusual metal abundances could explain the unusual large differences between trigonometric and spectral analysis results. More detailed abundance analyses of more PNNi would be needed to decide this question. In any case one conclusion is that even the metal blanketed atmospheres of Barstow et al. (2001) are not capable of producing results consistent with the trigonometric parallaxes.

The stellar parameters implied by the trigonometric parallax ($R = 0.025\ R_\odot$ or $\log g = 7.4$) places DeHt 5 at a location expected for a run-of-the-mill pre-white dwarf. The implied mass $M = 0.57\ M_\odot$ sits spot on the main peak of the white dwarf mass distribution ($M = 0.572$; Liebert et al. 2005). The implication is that DeHt 5 is a rather normal C/O white dwarf resulting from post-AGB evolution. Somewhat problematic is the high implied post-AGB age of $> 4 \times 10^5$ yr (read from the $0.605\ M_\odot$ track). The observational sample implies that PNe disperse into the interstellar medium after about (50–100) $\times 10^3$ yr (e.g., Table 1 in Napiwotzki 2001). A post-AGB age as high as implied for DeHt 5 would be highly unusual. Parker et al. (2006) speculate that DeHt 5 is not a real PNe, but a chance association of an interstellar cloud with a hot white dwarf. A more detailed investigation of the nebula will clarify this issue.

7. SUMMARY

HST FGS photometry indicates that none of these PNNi shows photometric variation larger than 5 mmag. From FGS interferometric fringe morphology, we establish companion limits mid-KV to early MV. FGS interferometric fringe tracking astrometry yields absolute trigonometric parallaxes for the PNNi of DeHt 5, Abell 31, NGC 7293, and NGC 6853. Weighted averages with previous ground-based determinations (Harris et al. 2007) provide parallaxes with errors at or below 0.2 mas, or $\langle \sigma_\pi / \pi \rangle = 5\%$. Our results confirm that statistical distances methods of the Shklovski type underestimate the distances of old planetary nebulae. On the other hand, the improved accuracy of our trigonometric parallaxes now show that previous spectroscopic distances significantly overestimated the distances. We see a consistent trend in the spectroscopic distance scale overestimating the true distance by 40% (corresponding to an underestimate of $\log g$ by 0.3 dex). Results from Napiwotzki (1999) and similar studies should be corrected accordingly. We use these parallaxes and estimates of interstellar extinction from

our own spectrophotometry and other investigations to derive PNNi absolute magnitudes. With these we derive radii, either comparing with the Sun through BCs, or with Vega via the V-band average flux, H_V. These four PNNi along with two others with well-determined distances and five WD satisfy theoretical linear correlations between absolute bolometric magnitude, log temperature, and log radius. Estimating from post-AGB evolutionary models, we find PNNi masses that agree with those typically found for white dwarf stars. The PNNi and the hottest WD clearly fall above a WD mass–radius relationship established by nearby, cool WD.

Support for this work was provided by NASA through grants NAG5-1603, GO-10432, and GO-10611 from the Space Telescope Science Institute, which is operated by AURA, Inc., under NASA contract NAS5-26555. These results are based partially on observations obtained with the Apache Point Observatory 3.5 m telescope, which is owned and operated by the Astrophysical Research Consortium. Washington/DDO photometry was secured at Las Campanas Observatory (Carnegie Institute of Washington) and Fan Mountain Observatory (University of Virginia). This publication makes use of data products from the Two Micron All Sky Survey, which is a joint project of the University of Massachusetts and the Infrared Processing and Analysis Center/California Institute of Technology, funded by NASA and the NSF. This research has made use of the SIMBAD database and Aladin, both developed at CDS, Strasbourg, France; the NASA/IPAC Extragalactic Database (NED) which is operated by JPL, California Institute of Technology, under contract with NASA; and NASA's Astrophysics Data System Abstract Service. We thank an anonymous referee for a careful reading and suggestions that improved the presentation.

REFERENCES

Barker, T. 1984, ApJ, 284, 589
Barstow, M. A., et al. 2001, MNRAS, 325, 1149
Barstow, M. A., et al. 2003, MNRAS, 341, 870
Barstow, M. A., et al. 2005, MNRAS, 362, 1134
Benedict, G. F., et al. 1998a, AJ, 116, 429
Benedict, G. F., et al. 1998b, in ASP Conf. Ser. 154, Cool Stars, Stellar Systems, and the Sun, ed. R. A. Donahue & J. A. Bookbinder (San Francisco, CA: ASP), 1212
Benedict, G. F., et al. 1999, AJ, 118, 1086
Benedict, G. F., et al. 2000, AJ, 119, 2382
Benedict, G. F., et al. 2002a, AJ, 124, 1695
Benedict, G. F., et al. 2002b, AJ, 123, 473
Benedict, G. F., et al. 2003, AJ, 126, 2549
Benedict, G. F., et al. 2007, AJ, 133, 1810
Bergeron, P., Wesemael, F., & Beauchamp, A. 1995, PASP, 107, 1047
Bessell, M. S., & Brett, J. M. 1988, PASP, 100, 1134
Bohlin, R. C., Harrington, J. P., & Stecher, T. P. 1982, ApJ, 252, 635
Bond, H. E. 2009, J. Phys. Conf. Ser., 172, 012029
Bond, H. E., & Livio, M. 1990, ApJ, 355, 568
Bradley, A., et al. 1991, PASP, 103, 317
Burstein, D., & Heiles, C. 1982, AJ, 87, 1165
Ciardullo, R., et al. 1999, AJ, 118, 488
Cox, A. N. 2000, Allen's Astrophysical Quantities (Melville, NY: AIP)
De Marco, O. 2009, PASP, 121, 316
Driebe, T., et al. 1999, A&A, 350, 89
Finley, D. S., Koester, D., & Basri, G. 1997, ApJ, 488, 375
Flower, P. J. 1996, ApJ, 469, 355
Franz, O. G., et al. 1998, AJ, 116, 1432
Girard, T. M., et al. 2000, AJ, 119, 2428
Hamada, T., & Salpeter, E. E. 1961, ApJ, 134, 683
Hanson, R. B. 1979, MNRAS, 186, 875
Harris, H. C., et al. 1997, in IAU Symp. 180, Planetary Nebulae, ed. H. J. Habing & H. J. G. L. M. Lamers (Dordrecht: Kluwer), 40
Harris, H. C., et al. 2007, AJ, 133, 631
Harrison, T. E., et al. 2004, AJ, 127, 460
Harrison, T. E., et al. 2009, AJ, 137, 4061
Holberg, J. B., et al. 1998, ApJ, 497, 935
Holberg, J. B., & Bergeron, P. 2006, AJ, 132, 1221
Hultzsch, P. J. N., et al. 2007, A&A, 467, 1253
Iben, I., Jr., & Renzini, A. 1983, ARA&A, 21, 271
Jefferys, W. H., Fitzpatrick, M. J., & McArthur, B. E. 1988, Celest. Mech., 41, 39
Kaler, J. B. 1983, ApJ, 271, 188
Kaler, J. B., Aller, L. H., & Czyzak, S. J. 1976, ApJ, 203, 636
Kawka, A., et al. 2008, ApJ, 675, 1518
Liebert, J., Bergeron, P., & Holberg, J. B. 2005, ApJS, 156, 47
Lutz, T. E., & Kelker, D. H. 1973, PASP, 85, 573
Majewski, S. R., et al. 2000, AJ, 120, 2550
Mauron, N., & Kendall, T. R. 2004, A&A, 428, 535
McArthur, B., et al. 2002, in The 2002 HST Calibration Workshop: Hubble after the Installation of the ACS and the NICMOS Cooling System, ed. S. Arribas, A. Koekemoer, & B. Whitmore (Baltimore, MD: STScI), 373
McArthur, B. E., et al. 2001, ApJ, 560, 907
Milne, D. K., & Aller, L. H. 1975, A&A, 38, 183
Napiwotzki, R. 1993, Acta Astron., 43, 343
Napiwotzki, R. 1999, A&A, 350, 101
Napiwotzki, R. 2001, A&A, 367, 973
Napiwotzki, R. 2006, A&A, 451, L27
Napiwotzki, R., & Rauch, T. 1994, A&A, 285, 603
Napiwotzki, R., & Schoenberner, D. 1995, A&A, 301, 545
Nelan, E. P. 2007, Fine Guidance Sensor Instrument Handbook (16th ed.; Baltimore, MD: STScI)
Nelan, E. P., et al. 2004, AJ, 128, 323
O'Brien, M. S., Bond, H. E., & Sion, E. M. 2001, ApJ, 563, 971
Palen, S., et al. 2002, AJ, 123, 2666
Paltoglou, G., & Bell, R. A. 1994, MNRAS, 268, 793
Parker, Q. A., et al. 2006, MNRAS, 373, 79
Phillips, J. P. 2005, MNRAS, 357, 619
Pottasch, S. R. 1996, A&A, 307, 561
Provencal, J. L., et al. 1998, ApJ, 494, 759
Provencal, J. L., et al. 2002, ApJ, 568, 324
Rauch, T. 2003, A&A, 403, 709
Savage, B. D., & Mathis, J. S. 1979, ARA&A, 17, 73
Schaefer, G., et al. 2006, BAAS, 38, 1104
Schlegel, D. J., Finkbeiner, D. P., & Davis, M. 1998, ApJ, 500, 525
Schönberner, D., & Blöcker, T. 1996, Ap&SS, 245, 201
Shipman, H. L., et al. 1997, ApJ, 488, L43
Shklovski, I. S. 1956, Sov. Astron. J., 33, 315
Soker, N. 2006, ApJ, 645, L57
Standish, E. M., Jr. 1990, A&A, 233, 252
Stanghellini, L., Shaw, R. A., & Villaver, E. 2008, ApJ, 689, 194
Stanghellini, L., et al. 2002, ApJ, 576, 285
Su, K. Y. L., et al. 2007, ApJ, 657, L41
van Altena, W. F., Lee, J. T., & Hoffleit, E. D. 1995, The General Catalogue of Trigonometric [Stellar] Parallaxes (4th ed.; New Haven, CT: Yale University Observatory)
van Leeuwen, F. 2007, Astrophysics and Space Science Library Vol. 350, Hipparcos, the New Reduction of the Raw Data (Berlin: Springer)
Werner, K. 1996, ApJ, 457, L39
Zacharias, N., et al. 2004, AJ, 127, 3043